Tidal mixing maintains regional differences in water properties and nutrient ratios in British Columbia coastal waters

Hayley V. Dosser[1], Stephanie Waterman[1], Jennifer M Jackson[2], Charles Hannah[3], and Brian P. V. Hunt[1]

[1]University of British Columbia
[2]Hakai Institute
[3]Institute of Ocean Sciences

November 21, 2022

Abstract

Tidal mixing is recognized as a key mechanism in setting water properties in coastal regions globally. Our study focuses on Canada's British Columbia coastal waters, from Queen Charlotte Strait to the Strait of Georgia. This area is bisected by a region of exceptionally strong mixing driven by some of the strongest tidal currents in the world. We examine the influence of this tidal mixing on regional differences in water properties and nutrient ratios. Our results quantify a spatially-abrupt and temporally-persistent lateral gradient in temperature, salinity, and density co-located with the region of strongest mixing. The distributions of density on either side of this front remain largely distinct throughout the spring-neap tidal cycle, year-round, and for over 70 individual years for which data are available. Additionally, nutrient molar ratios north of the front are statistically distinct from those to the south. Seasonal changes driven by the arrival of upwelled water differ in both timing and magnitude on either side of the front. Taken together, these results indicate limited exchange of water through the region of strongest tidal mixing, and suggest that Queen Charlotte Strait and the Strait of Georgia are largely isolated from each other. As such, this area provides a valuable case study for the degree to which the reduction of estuarine exchange by tidal mixing can maintain abrupt and substantial regional differences in physical and biogeochemical water properties. Further, it demonstrates the potential of tidal mixing to modify nutrient transport pathways, with implications for marine ecosystems.

Tidal mixing maintains regional differences in water properties and nutrient ratios in British Columbia coastal waters

H. V. Dosser[1], S. Waterman[1], J. M. Jackson[2], C. G. Hannah[3], B. P. V. Hunt[1,4,5]

[1]Department of Earth, Ocean and Atmospheric Sciences, University of British Columbia, Vancouver, BC, V6T 1Z4
[2]Hakai Institute, 1010 Langley St, Victoria, BC, V8W 1V8
[3]Fisheries and Oceans Canada, Institute of Ocean Sciences, Sidney, BC, V8L 4B2
[4]Institute for the Oceans and Fisheries, University of British Columbia, Vancouver, BC, V6T 1Z4
[5]Hakai Institute, Heriot Bay, Quadra Island, BC, V0P 1H0

Key Points:

- An abrupt and persistent lateral gradient in water properties is quantified, co-located with strong tidal mixing bisecting the study area.
- Differences in the seasonality, open-ocean connectivity, and response to stressors are found in the regions separated by the tidal mixing.
- The mixing is likely limiting the two-layer estuarine exchange flow between regions, and so modifying the transport pathways for nutrients.

Corresponding author: Hayley V. Dosser, `hdosser@eoas.ubc.ca`

Abstract

Tidal mixing is recognized as a key mechanism in setting water properties in coastal regions globally. Our study focuses on Canada's British Columbia coastal waters, from Queen Charlotte Strait to the Strait of Georgia. This area is bisected by a region of exceptionally strong mixing driven by some of the strongest tidal currents in the world. We examine the influence of this tidal mixing on regional differences in water properties and nutrient ratios. Our results quantify a spatially-abrupt and temporally-persistent lateral gradient in temperature, salinity, and density co-located with the region of strongest mixing. The distributions of density on either side of this front remain largely distinct throughout the spring-neap tidal cycle, year-round, and for over 70 individual years for which data are available. Additionally, nutrient molar ratios north of the front are statistically distinct from those to the south. Seasonal changes driven by the arrival of upwelled water differ in both timing and magnitude on either side of the front. Taken together, these results indicate limited exchange of water through the region of strongest tidal mixing, and suggest that Queen Charlotte Strait and the Strait of Georgia are largely isolated from each other. As such, this area provides a valuable case study for the degree to which the reduction of estuarine exchange by tidal mixing can maintain abrupt and substantial regional differences in physical and biogeochemical water properties. Further, it demonstrates the potential of tidal mixing to modify nutrient transport pathways, with implications for marine ecosystems.

Plain Language Summary

Mixing caused by the tides affects properties in coastal waters globally. Our study focuses on coastal waters in British Columbia Canada, from Queen Charlotte Strait to the Strait of Georgia. This area is bisected by a region of strong mixing caused by some of the strongest tidal currents in the world. We examine how this tidal mixing affects water properties. Our results show that temperature, salinity, density, and the relative proportions of key nutrients change significantly across the region of strongest mixing. These differences between the two halves of the study area persist throughout the tidal cycle and year-round, for over 70 individual years. We also find differences in the seasonal cycles in properties and their similarity to open ocean waters. These results indicate that the exchange of water through the region of strongest tidal mixing is significantly limited, which suggests that Queen Charlotte Strait and the Strait of Georgia

are largely isolated from each other. As such, this area provides a valuable case study for the ability of tidal mixing to maintain abrupt and substantial regional differences in water properties. Further, it suggests that tidal mixing can affect nutrient transport to different regions, an important consideration for marine ecosystems.

1 Introduction

Tidal mixing has been widely shown to play an important role in the modification of coastal water properties and the maintenance of persistent tidal fronts, leading to distinct physical and biogeochemical properties in adjacent regions (Thomson, 1981; LeBlond, 1983; van Heijst, 1986; Loder et al., 1994). In many cases, tidal mixing can limit the estuarine exchange flow typical of coastal waters (e.g. Waldichuk, 1957; Griffin & LeBlond, 1990; Masson, 2002; MacCready & Geyer, 2010; Johannessen et al., 2014) reducing the transport of properties between regions. The resulting regional differences in water properties have direct effects on marine ecosystem function, including primary and secondary productivity, the location of biological hotspots, and the connectivity of ecosystems (Harrison et al., 1983; Gay & Vaughan, 2001; Arimitsu et al., 2016).

The influence of tidal mixing is expected to be particularly significant on the southwestern coast of British Columbia (BC) Canada, an area where rapid tidal currents and complex topography force some of the strongest tidally-driven turbulence in the world (e.g. Foreman et al., 2012). Our specific study area along the BC coast is located to the east and north of Vancouver Island; from eastern Queen Charlotte Strait (QCSt) through Johnstone Strait (JS) and the Discovery Islands (DI) into the northern Strait of Georgia (SoG) (Figure 1). Strong tidal currents in the study area are well-documented, as is the resulting intense turbulent mixing over rough bathymetry and sills (Thomson, 1981; Griffin & LeBlond, 1990; Foreman et al., 2004). In particular, the shallow, narrow channels in eastern JS and the DI that bisect the study area are known to have the strongest tidal currents in Canada, driving the most intense turbulence in Canadian waters (Whitney et al., 2005).

Southwestern British Columbia's complex topography was carved out by glaciers, and is characterized by fjords, islands, inlets and straits. The tidal currents are mixed, dominantly semidiurnal, and propagate both north and south around Vancouver Island before meeting in the area between QCSt and the SoG (Thomson, 1981). A two-layer

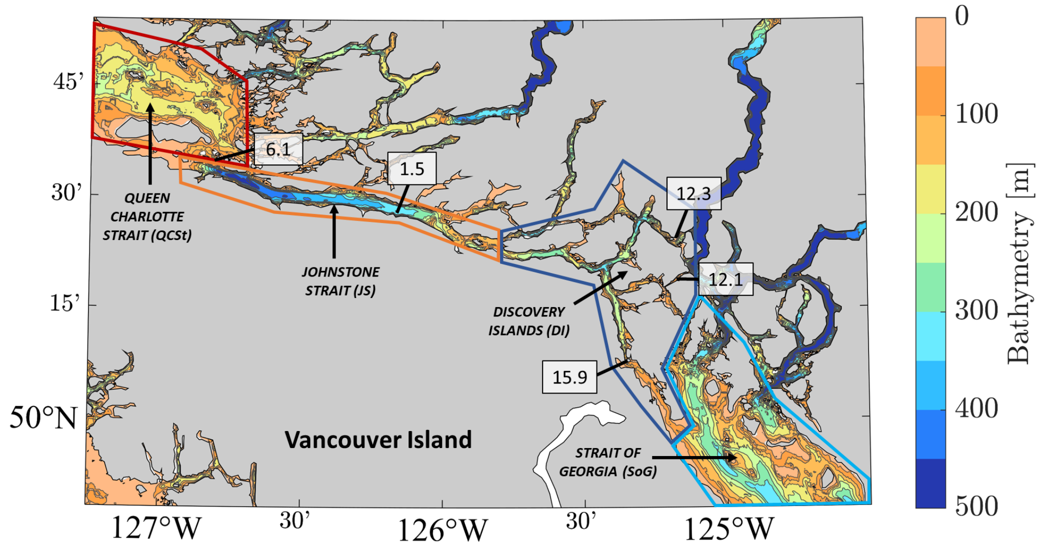

Figure 1. Bathymetric map of the study area showing the boundaries of the four regions: eastern Queen Charlotte Strait (QCSt, red), western Johnstone Strait (JS, orange), the Discovery Islands region (DI, dark blue), and the northern Strait of Georgia (SoG, light blue). The maximum tidal currents (in knots) in select passages are given (*Canadian Tide and Current Tables / Tables des marées et courants du Canada*, 2019).

estuarine circulation is driven by surface outflow from numerous terrestrial freshwater sources, with stratification in the area controlled primarily by salinity. Reviews of the physical oceanography of the area are provided by Thomson (1981); LeBlond (1983); Whitney et al. (2005) and Riche et al. (2014). Similar complex coastal marine environments are encountered in Alaska, the south-west coast of Chile, New Zealand, and Scandinavia (e.g. Stanton & Pickard, 1980; Svendsen, 1995; Iriarte et al., 2014; Arimitsu et al., 2016).

Biological productivity in British Columbia's coastal waters is driven in part by the coastal upwelling of nutrient-rich deep ocean waters (Ware & McFarlane, 1989; Whitney et al., 2005). Specifically, nutrients in these coastal waters are replenished seasonally when large-scale wind patterns shift from downwelling- to upwelling-favorable, driving a deep inflow of water from the Northeast Pacific Ocean. Nutrient molar ratios in these coastal waters can differ significantly from open ocean values due to modification by e.g., riverine inputs and denitrification in anoxic sediments (Smethie, 1987; Whitney et al., 2005). The influence of such modification is expected to vary regionally, partially as a result of tidal mixing limiting two-layer estuarine exchange flow and driving vertical transport of nutrients towards the euphotic zone. Regional variations in the ratios of nitrate, phosphate, and silicate can have significant implications for phytoplankton species composition and productivity (Geider & La Roche, 2002; Arrigo, 2005; Strom et al., 2006; Klausmeier et al., 2008).

An important effect of extremely vigorous tidal mixing on the circulation is to remove momentum from the two-layer estuarine exchange flow and enhance vertical momentum transfer (Griffin & LeBlond, 1990; Hibiya & LeBlond, 1993; Park & Kuo, 1996; MacCready, 1999), causing a recirculation of inflowing water. In nearby Haro Strait, tidal mixing is known to periodically drive such a recirculation, limiting estuarine exchange and restricting deep inflow to occasional pulses of dense water passing over the sill between the Strait of Georgia and the Strait of Juan de Fuca (Griffin & LeBlond, 1990; LeBlond et al., 1991; Hibiya & LeBlond, 1993; Masson, 2002; Masson & Cummins, 2004; Johannessen et al., 2014). The impact of tidal mixing on circulation in our study area is expected to be even more pronounced, making this area an ideal case study for the potential of tidal mixing to drive sustained regional differences in physical and biogeochemical water properties. Past studies by Thomson (1976) and Thomson (1981) showed evidence of such a transition in properties in the study area, identifying a well-defined full-depth density front co-located with the sill separating the shallower eastern end of JS from the DI. The reduction of estuarine exchange, the recirculation of inflowing water, and other impacts of tidal mixing are additionally expected to result in region-specific ecosystem dynamics and responses to environmental stressors that presently affect the study area, including ocean acidification (e.g. Feely et al., 2016; Evans et al., 2019), hypoxia (e.g. Crawford & Peña, 2013), and marine heatwaves (e.g. Di Lorenzo & Mantua, 2016; Jackson et al., 2018).

In this study, our goal is to robustly quantify regional differences in water properties and consider the implications for eastern Queen Charlotte Strait through to the northern Strait of Georgia, transecting the region of intense tidal mixing in Johnstone Strait and the Discovery Islands. To do so, we combine historic observations spanning multiple decades with high-temporal resolution observations from recent years, thereby creating a new regional data product for physical water properties and nutrient concentrations (Section 2). We use this data product to quantify spatial and temporal variability in water properties to a previously inaccessible degree (Section 3), creating a comprehensive picture of the regional structure of physical water properties and nutrient ratios. Finally, we discuss how these findings provide insight into the role of tidal mixing in setting coastal ocean properties and maintaining regional separation, and further how this mixing-induced regionalization can impact ecosystems (Section 4).

2 Data and Methods

From this point onwards, the abbreviations QCSt, JS, DI, and SoG will be used to refer to the four regions shown in Figure 1. These useful subdivisions of our study area are defined based on data availability, bathymetric features such as sills that provide natural boundaries, and stratification used as a proxy for the influence of mixing in each region (see Supporting Information S.1 for a full discussion). In these regions, the far eastern end of Johnstone Strait is included in the DI region, so that 'JS' refers strictly to the western part of Johnstone Strait outlined in Figure 1. As such, the density front in Johnstone Strait described in Thomson1976 and Thomson1981 and discussed herein is co-located with the sill separating the JS and DI regions. We refer to this transition zone between JS and the DI as the 'tidal mixing frontal zone'.

2.1 Data sources

We quantify the spatial and temporal variability of physical and biogeochemical water properties in the study area through the creation and analysis of a new data product combining archived temperature (T), salinity (S), and nutrient concentration data spanning multiple decades (Figure S2) collected by Fisheries and Oceans Canada (DFO) and the University of British Columbia (UBC) with more recent data collected at high temporal resolution by the Hakai Institute (Hakai). Details on these data sources are given below and in Supporting Information S.2. Our analysis represents the first time that data from these sources have been combined for this geographic area. The resulting data product provides a combination of unparalleled spatial and temporal coverage over the regions of interest, with sufficient temporal resolution in each region to investigate seasonal variability in water properties (Figures S1, S2).

DFO has collected hydrographic temperature and salinity data in QCSt, JS, the DI, and the SoG since the 1930s (*Institute of Ocean Sciences Data Archive*, 2020). Additionally, UBC has collected hydrographic data in the study area since the 1970s. These historic data were collected at locations spread across the study area during all months of the year. In total, 3,269 DFO profiles and 1,138 UBC profiles are included in the new data product and our analysis. Of these, 608 are from QCSt, 1,522 are from JS, 872 are from the DI, and 1,405 are from the SoG. From the 1930s to the mid-1970s, temperature was measured using a reversing thermometer, while salinity was measured from water samples. Beginning in the mid-1970s, use of a Conductivity-Temperature-Depth (CTD) instrument equipped with electronic sensors to measure temperature, conductivity, and pressure became common. The accuracy of the archived measurements is at minimum 0.1°C for temperature and 0.1 for CTD salinity. Salinity data collected pre-1980 using bottle samples is comparable to recent CTD-based salinity data with an accuracy of 0.4 (Chandler et al., 2017).

More recently, from 2014 to present, the Hakai Institute has collected CTD data in QCSt near the sill with JS, in the deep western end of JS, in the DI, and in the northern SoG near Quadra Island where a Hakai field station is located. A total of 3,131 Hakai CTD profiles are included in the data product and our analysis: this includes 103 profiles in QCSt, 244 profiles in JS, 353 profiles in the DI, and 2,431 profiles in the SoG. The accuracy of these measurements is 0.005°C or better for temperature and 0.001 or better for salinity.

Nutrient concentration data (nitrate+nitrite, phosphate, and silicate) collected by DFO since 1977 are also included in our analysis (*Institute of Ocean Sciences Data Archive*, 2020). We use a total of 334 DFO nutrient profiles, with 48 profiles from QCSt, 46 profiles from JS, 61 profiles from the DI, and 179 profiles from the SoG. Here a 'profile' refers to a set of samples collected at a single location for all three nutrients. Sample precision is estimated to be 0.2 μmol L^{-1} or better for nitrate+nitrite, 0.03 μmol L^{-1} or better for phosphate and 0.4 μmol L^{-1} or better for silicate. Nutrient samples are not filtered and were processed fresh until recent years, now most samples are processed frozen.

The DFO nutrient data are combined with Hakai Institute nitrate+nitrite, phosphate, and silicate concentration data collected at repeat sampling stations. These data are available from 2014 onwards. A total of 909 Hakai nutrient profiles are used in the analysis, with 102 profiles in QCSt, 189 profiles in JS, 79 profiles in the DI, and 539 profiles in the SoG. Sample precision is estimated to be 0.2 μmol L^{-1} or better for nitrate+nitrite (hereafter 'nitrate'), 0.02 μmol L^{-1} or better for phosphate and 0.2 μmol L^{-1} or better for silicate. Nutrient collection and processing protocols are identical to those currently used by DFO, with the exception that nutrients are filtered and are often collected by small boat and so kept upright on ice in a cooler until they can be frozen to -20°C.

2.2 Data interchangeability and sampling bias

Our analysis of the new combined data product has the goals of quantifying persistent regional differences in physical water properties and nutrient ratios, as well as resolving seasonal and depth variability in these regions. As such, interchangeability of data from different sources is necessary, as is a careful consideration of biases in sampling.

The DFO, UBC, and Hakai data collection programs are independently run, and the DFO data includes measurements collected by different internal programs (further details provided in Chandler et al. (2017) and Supporting Information S.2). Previous studies that considered both DFO and Hakai hydrographic data sets suggest that the data are comparable and can be used interchangeably (e.g. Jackson et al., 2018). Preliminary comparisons (not shown) between nutrient samples collected by Hakai and DFO within several days of each other at nearby locations suggests these data can also be used interchangeably.

Due to the realities of sampling conducted over decades by multiple agencies, significant interannual, seasonal, depth, and spatial biases are present in the combined data product and must be considered. A detailed description of known biases is provided in Supporting Information S.2; a brief discussion of the ways in which we designed our analysis to minimize these biases in our results follows below. Biases for nutrient data are similar to those for temperature and salinity, and we note that the number of nutrient samples is relatively low compared to the number of hydrographic profiles (Figure S2). As the variables considered herein are frequently not normally distributed, we characterize the 'average' of a distribution of values using the median rather than the mean, unless otherwise specified.

Owing to interannual bias in sampling, which varies by region (Figure S2), our analysis does not include an examination of interannual trends. Rather, we focus on the persistence of regional differences over the full duration of the data record. Seasonal bias in sampling is present in all regions due to the difficulty of making measurements during winter conditions, though this is particularly notable in the QCSt and JS regions (Figure S3). In cases where this seasonal bias is likely to significantly impact our analysis, data are averaged monthly or grouped into summer (May to October) vs. winter (November to April) periods.

Our analysis examines both the fresh upper and dense lower layer in the two-layer estuarine exchange flow present in much of the study area, necessitating consideration of depth biases in sampling. For consistency between the physical and nutrient data, we calculate the mean value of temperature, salinity, and nutrient concentration data in 25 m bins for most of the analysis. When appropriate, we focus on differences between the 'upper' ($<$50 m depth) and 'lower' ($\geq$50 m depth) portions of the water column. The top 10 m of T and S profiles are excluded from much of the analysis due to higher uncertainty and the relative scarcity of surface measurements (Supporting Information S.2).

To minimize the impacts of spatial biases in sampling on our results, we focus on identifying robust large-scale inter-regional variations. In doing this, we make the implicit assumption that variations of water properties within regions (whether captured by our data or not) are smaller than variations between regions. The results herein support this assumption for locations where profiles are available. Nutrient data are spatially sparse (Figure S4), and a concerted observational effort would be required to accurately quantify smaller-scale spatial variations in nutrient concentrations within each region.

We acknowledge that it is not possible to fully eliminate the impacts of sampling bias on our analysis. Our aims are to design our analysis to minimize these impacts to a reasonable extent and to interpret our results within the context of the known biases described above.

3 Results

In what follows, we use the combined data product to quantify regional differences in water properties, which are sustained by the strong tidal mixing in the tidal mixing frontal zone. We examine the spatial and temporal variability of water properties by region, and quantify a spatially-abrupt and temporally-persistent transition within this frontal zone. We show that, despite their geographic proximity, the physical water properties, nutrient ratios, and seasonality in QCSt and JS are distinct from those in the northern SoG and the DI.

3.1 Stratification and inferred tidal mixing strength

While we do not measure ocean currents or mixing directly, we use the stratification in the upper water column as a qualitative proxy to infer the relative strength and delineate the spatial extent of the tidal mixing in each region within the study area. We assume that mixing in this area is primarily tidally-driven based both on previous studies (e.g. Thomson, 1981; Griffin & LeBlond, 1990; Foreman et al., 2004) and on the strong tidal currents present in the JS and DI regions (Figure 1, *Canadian Tide and Current Tables / Tables des marées et courants du Canada* (2019)). We characterize the stratification using the average buoyancy frequency, N^2, in the upper 50 m of the water column (Figure 2, Supporting Information S.1). Our characterization indicates that the strongest tidal mixing occurs in the DI, where the near-homogenization of the water column is immediately apparent. Relatively weak stratification in the JS region suggests weak tidal mixing there, while relatively strong stratification in QCSt and the SoG suggests minimal or absent tidal mixing in these regions. Regional differences in stratification are similar in summer and winter, with lower values of N^2 overall in winter (Figure S1). Based on these results, we infer that the majority of the tidal mixing occurs in JS and the DI during all seasons. We focus our analysis on regional differences and the transition in properties across the tidal mixing frontal zone (Figure 1), however we note that strong mixing is also known to occur at locations in JS and the DI outside of this zone.

3.2 Temperature and salinity contrast

To investigate how the tidal mixing frontal zone is linked to a transition in water properties, we first examine regional differences in temperature and salinity data (Figure 3). A temperature-salinity (T-S) diagram for JS and the DI (Figure 3, right inset) reveals an abrupt, distinct, and persistent regional contrast in T-S properties, evident in the clear separation between the two regions in T-S space. This abrupt transition between JS and the DI occurs roughly along the 1023 kg m^{-3} isopycnal. Geographically, this transition bisects the study area and the regional differences in properties remain visible in the adjacent regions: temperature and salinity values in QCSt are distinct from those in the SoG (Figure 3, left inset). Specifically, T-S properties in JS are similar to upper ocean waters in QCSt (density <1025.0 kg m^{-3}), while properties in the DI resemble those of upper ocean waters in the SoG (density <1023.0 kg m^{-3}) (Figure 3 insets, density contours). The QCSt/JS regions have T-S properties that more closely re-

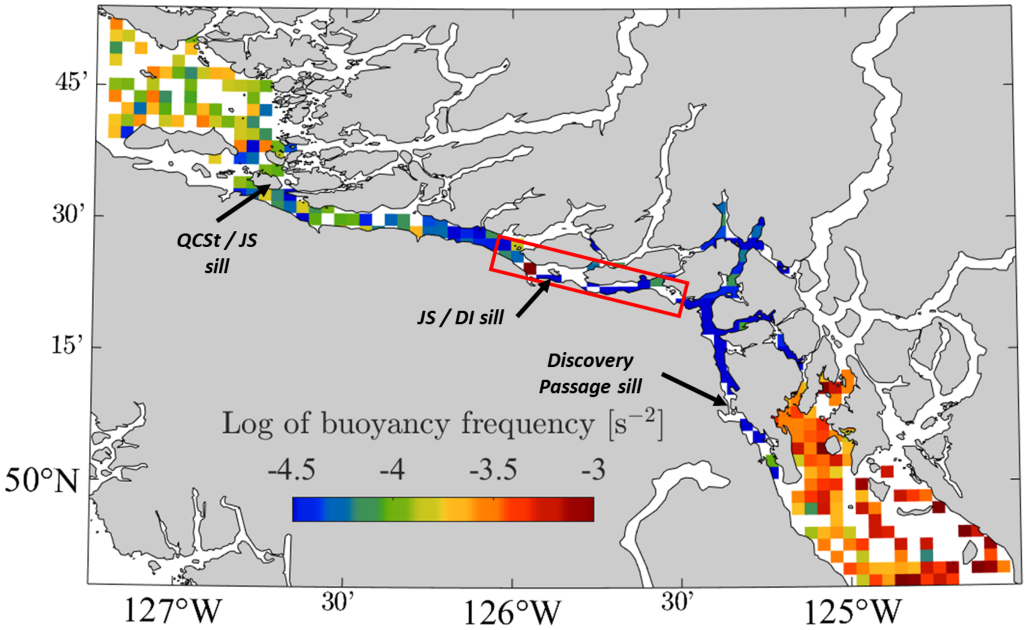

Figure 2. Log of buoyancy frequency, N^2 (in s^{-2}), in the upper 50 m of the water column, calculated from 2 m vertically-binned temperature and salinity profile data, with the median value for May to October shown. Within each 2.5 km square grid box, a median value for each month is calculated, then the median value of the summer months is determined. White grid boxes are locations with no data available, or outside the study area. Winter months (Figure S1) display similar regional differences but lower stratification overall. The approximate locations of shallow sills mentioned in the text are indicated, as is the tidal mixing frontal zone (red box).

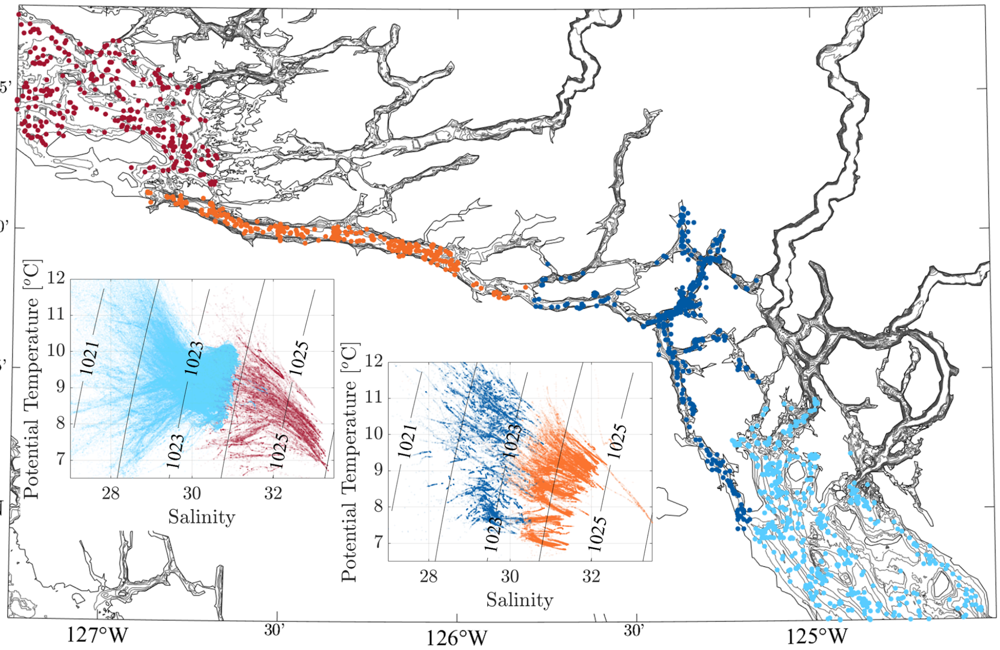

Figure 3. (Map) Locations of hydrographic profiles coloured by region, with QCSt in red, JS in orange, the DI in dark blue and the SoG in light blue. (Insets) Temperature-salinity diagrams for all potential temperature and salinity profile data from the locations on the map, coloured by region. Data have not been binned or averaged. Black lines give contours of potential density.

semble values seen in the open Northeast Pacific Ocean adjacent to the BC continental shelf (e.g. Thomson & Krassovski, 2010), whereas the SoG/DI regions are warmer and fresher year-round. The relatively cooler and more saline waters in QCSt and JS relative to the SoG and DI may thus reflect their proximity and higher connectivity to the open ocean.

An examination of the average seasonal cycles in the upper (10-50 m depth) and lower (50-200 m depth) water column (Figure 4) allows us to assess seasonal variability in this regional T-S contrast. Regional differences in salinity are roughly constant year-round in the upper water column (Figure 4a). In contrast, there is a summer increase in salinity in the lower water column (Figure 4b) seen only in QCSt and JS caused by seasonal upwelling, discussed in Section 3.4. In the upper water column, the median salinity in the SoG is 2.2 units fresher than in QCSt, while median salinity in the DI region is 1.4 units fresher than in JS. The largest regional difference in the upper water column occurs in August, when the SoG and DI are 2.6 units fresher than QCSt. In the lower

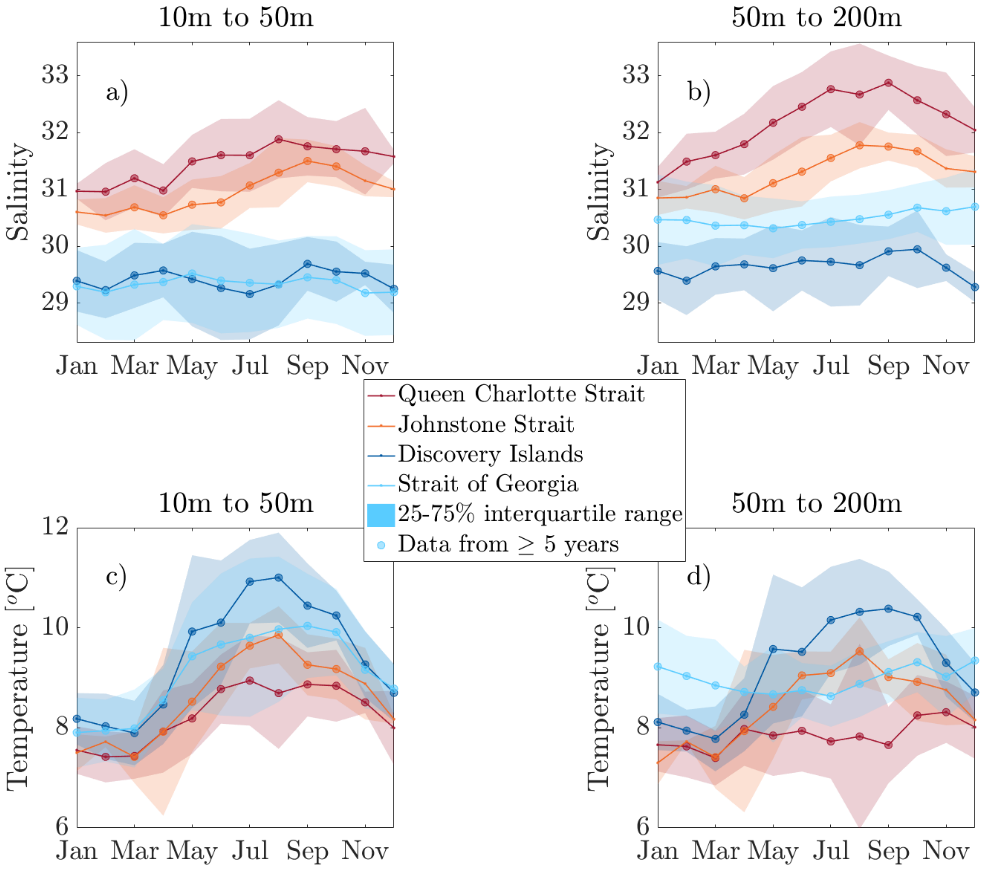

Figure 4. A comparison of regional seasonal cycles in a) salinity from 10-50 m depth, b) salinity from 50-200 m depth, c) potential temperature from 10-50 m depth, and d) potential temperature from 50-200 m depth. Lines give median monthly values for data from all available years with dots indicating months with data from 5 or more years. Shaded envelopes give the 25-75% interquartile range. Colour corresponds to region as indicated in the legend.

water column, median salinity in the SoG is 1.9 units fresher than in QCSt, and median salinity in the DI region is 1.5 units fresher than JS. The largest regional difference occurs in July, when the DI is 3.0 units fresher than QCSt. The reduced salinity contrast between the upper and lower water column in JS and the DI region, relative to that in the SoG and QCSt, is likely due to homogenization of the deep waters with the overlying surface layers through strong tidal mixing. Consistent with this picture, the freshest and warmest deep waters are in the DI, where the strongest tidal mixing occurs.

Regional temperature differences are also present year-round. The magnitude of the temperature contrast between regions varies seasonally in both the upper and lower portions of the water column. In the upper water column (Figure 4c), temperatures in summer (May to October) in the SoG and DI are often 1-2°C warmer than in QCSt and JS, though variations between months are large. The largest regional difference occurs in August, when the DI is 2.3°C warmer than QCSt. Regional temperature differences in the upper water column in winter (November to April) are generally much smaller (typically less than 1°C), reflecting the influence of large-scale atmospheric conditions that span the study area as a whole. In the lower water column (Figure 4d), temperatures in the SoG and QCSt display less seasonal variation, with temperatures in the SoG roughly 1°C warmer than QCSt year-round. In contrast, JS and the DI show a pronounced seasonal cycle matching that in the upper water column. The largest regional difference occurs in September, when the DI is 2.7°C warmer than QCSt. Minimal variation in temperature between the upper and lower water column in JS and the DI is likely due to the strong vertical mixing characteristic of these regions.

3.3 Density contrast

In BC coastal waters, density is primarily but not solely controlled by salinity, and so displays a persistent lateral gradient similar to that in salinity within the regions of strongest tidal mixing. The temperature and salinity contrasts detailed above result in ranges of potential density values in QCSt and JS that rarely overlap with those observed in the SoG and DI, in both the upper (10-50 m depth) and lower ($\geq$50 m depth) water column (Figure 5). The densest water is found deep in QCSt, and the lightest at the surface in the SoG. The lightest water in QCSt (JS) is denser than the densest water in the SoG (DI) for the large majority of observations. The density distributions in JS vs. the DI and in QCSt vs. the SoG thus have minimal overlap and are statistically distinct at

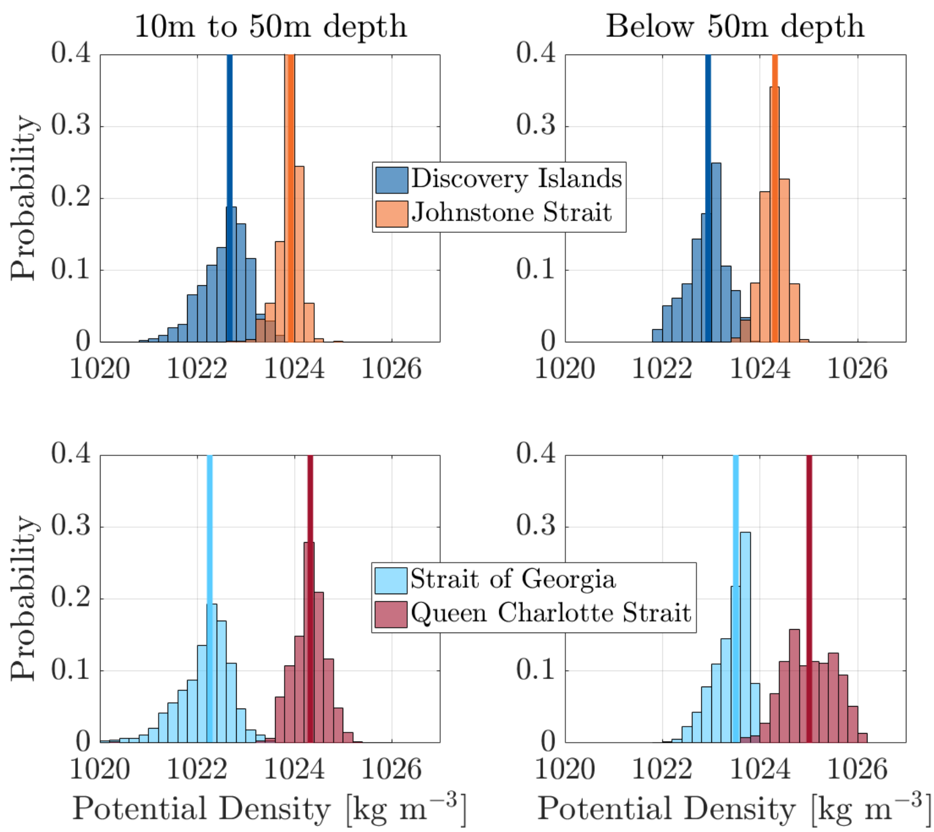

Figure 5. Regional distributions of potential density calculated using the full temperature and salinity dataset, binned every 25 m in the vertical, for the upper 10-50 m depth of the water column (left) and below 50 m depth (right). Vertical lines give the median value of density in each distribution.

the 99% confidence level ($p<0.001$) using a Kolmogorov-Smirnov test ("Kolmogorov–Smirnov Test", 2008), which is used to determine the likelihood that two separate distributions of data are drawn from the same overall distribution.

The inclusion of year-round temperature and salinity profile data spanning 1932 to 2018 demonstrates that this transition in density persists between seasons and interannually, for all months and for the 70 individual years for which data are available. An examination of near full-depth profile data confirms that these properties change rapidly in the horizontal at all subsurface depths (see Section 4.1 for further details). Additionally, this transition is present during both the spring and neap phases of the fortnightly tidal cycle. To confirm that both spring and neap tides are well-sampled in all regions, we note that samples are collected with weekly or higher frequency for 39% of days sam-

	QCSt	JS	DI	SoG
	Nutrient concentration (μmol L^{-1})			
Nitrate	23 ± 6	23 ± 5	25 ± 4	29 ± 5
Phosphate	1.9 ± 0.5	1.9 ± 0.4	2.2 ± 0.3	2.5 ± 0.4
Silicate	38 ± 14	39 ± 12	49 ± 9	54 ± 10
	Nutrient molar ratio			
N:P	12.3 ± 0.8	12.2 ± 1.0	11.4 ± 1.1	11.3 ± 1.0
N:Si	0.59 ± 0.08	0.58 ± 0.06	0.51 ± 0.03	0.51 ± 0.06
P:Si	0.048 ± 0.005	0.048 ± 0.005	0.045 ± 0.005	0.045 ± 0.005

Table 1. Median values and the 25-75% interquartile ranges for full-depth nutrient concentrations and nutrient molar ratios in each region. The median and interquartile range are given, rather than the mean and standard deviation, as the data are not normally distributed. For comparison, Redfield-Brzezinski values are 16 for N:P, 1.1 for N:Si, and 0.07 for P:Si.

pled in QCSt, 54% in JS, 34% in the DI, and 66% in the SoG. Full-depth density profiles on either side of the tidal mixing frontal zone have no notable differences during spring vs. neap tides (not shown). This lack of evidence for significant spring-neap modulation of the density structure across the tidal mixing frontal zone is significant. Spring-neap modulation of the residual circulation is a well-known indicator of tidal mixing (Hibiya & LeBlond, 1993; Park & Kuo, 1996; MacCready et al., 2018), and its apparent absence here suggests that the strength and spatial extent of the tidal mixing may be sufficient to permanently disrupt the two-layer estuarine exchange flow within the tidal mixing frontal zone (tidal currents remain above 75 cm s^{-1} at some locations in the DI even during low neap tides). However, more measurements within the tidal mixing frontal zone would be needed to fully analyze tidal modulation of the mixing front.

3.4 Contrast in nutrient molar ratios

In addition to the regional separation in physical water properties, there are statistically significant differences in nutrient molar ratios between the QCSt/JS and SoG/DI regions. Regional distributions of the molar ratio of nitrate to phosphate (Figure 6), nitrate to silicate (Figure 7), and phosphate to silicate (Figure 8) are examined for both the upper (<50 m depth) and lower (≥50 m depth) water column. Median values and interquartile ranges for nutrient concentrations and nutrient molar ratios for each region

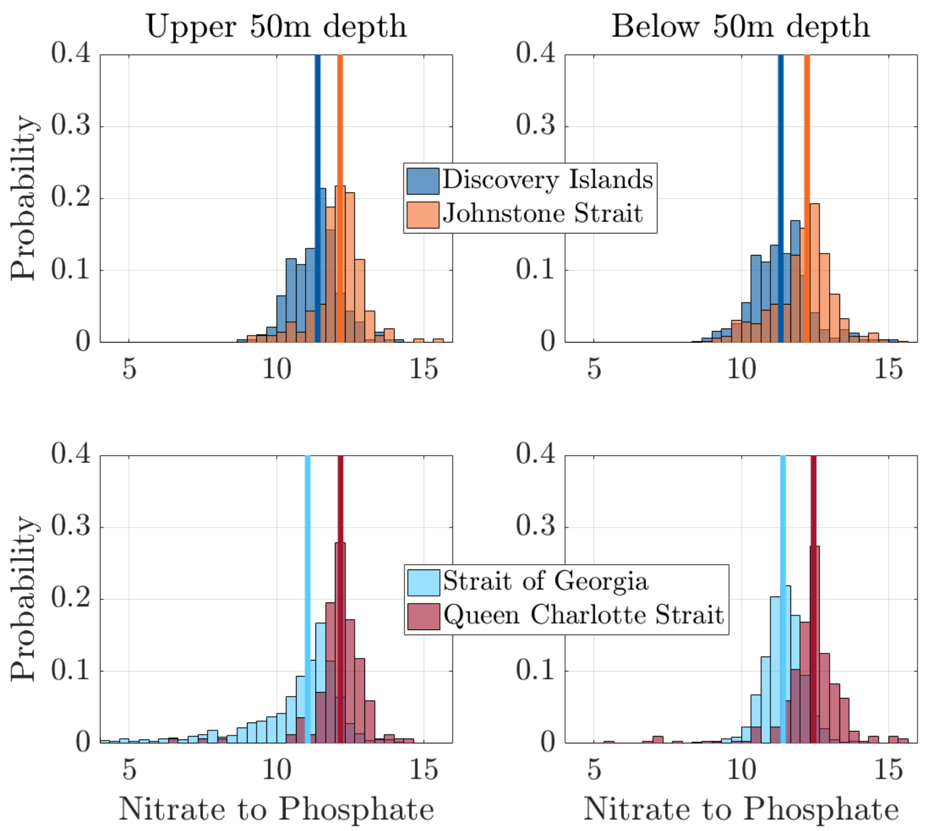

Figure 6. Regional distributions of the nitrate to phosphate molar ratio, calculated using the full nutrient dataset, binned every 25 m in the vertical, for the upper 50 m depth of the water column (left) and below 50 m depth (right). Vertical lines give the median value for each distribution.

are given in Table 1. Nutrient ratios are assessed relative to the Redfield-Brzezinski molar ratios for carbon to silicon to nitrogen to phosphorus (Brzezinski, 1985), which are canonically C:Si:N:P = 106:15:16:1 in open-ocean waters. Our nutrient ratios are generally lower in all regions than these canonical open-ocean values (Table 1). Median values of the nutrient ratios in both the upper and lower water column are closest to canonical open-ocean values in QCSt and JS, and differ most significantly from canonical open-ocean values in the SoG and DI.

Median values for the molar ratio of nitrate to phosphate (N:P, Figure 6) vary from 11.3 in the SoG to 12.3 in QCSt (Table 1), an 8% difference. The largest regional difference is for the nitrate to silicate ratio (N:Si, Figure 7), with a 14% difference between the median value of 0.59 in QCSt and 0.51 in the SoG and DI (Table 1). The phosphate

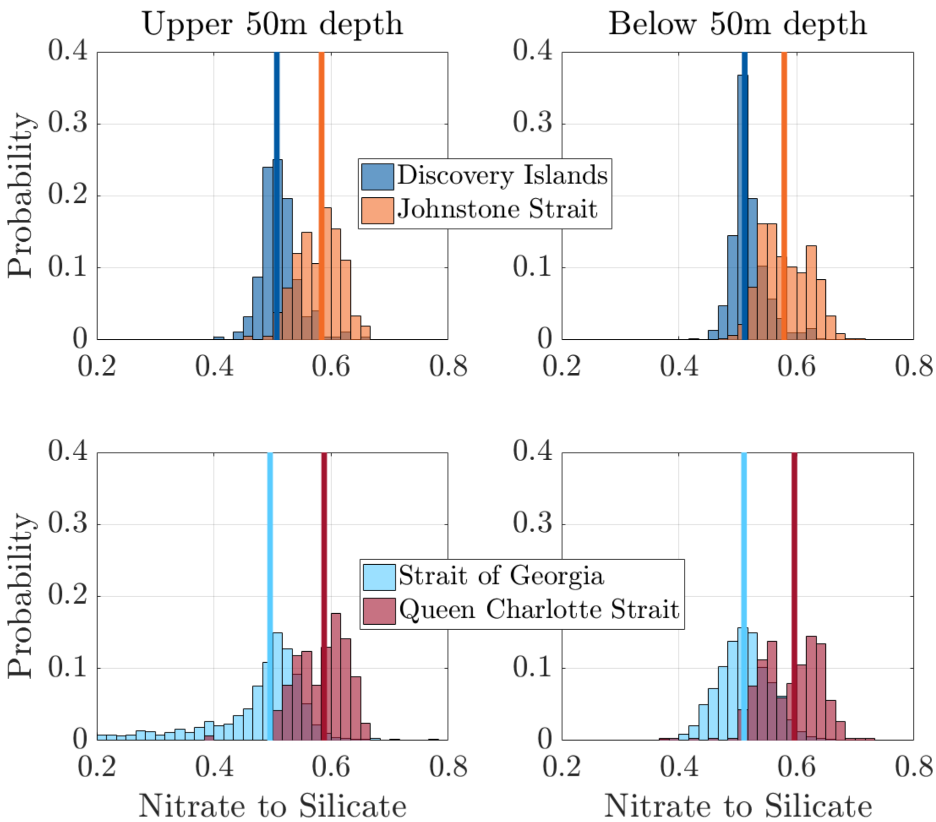

Figure 7. As in Figure 6, but for the molar ratio of nitrate to silicate.

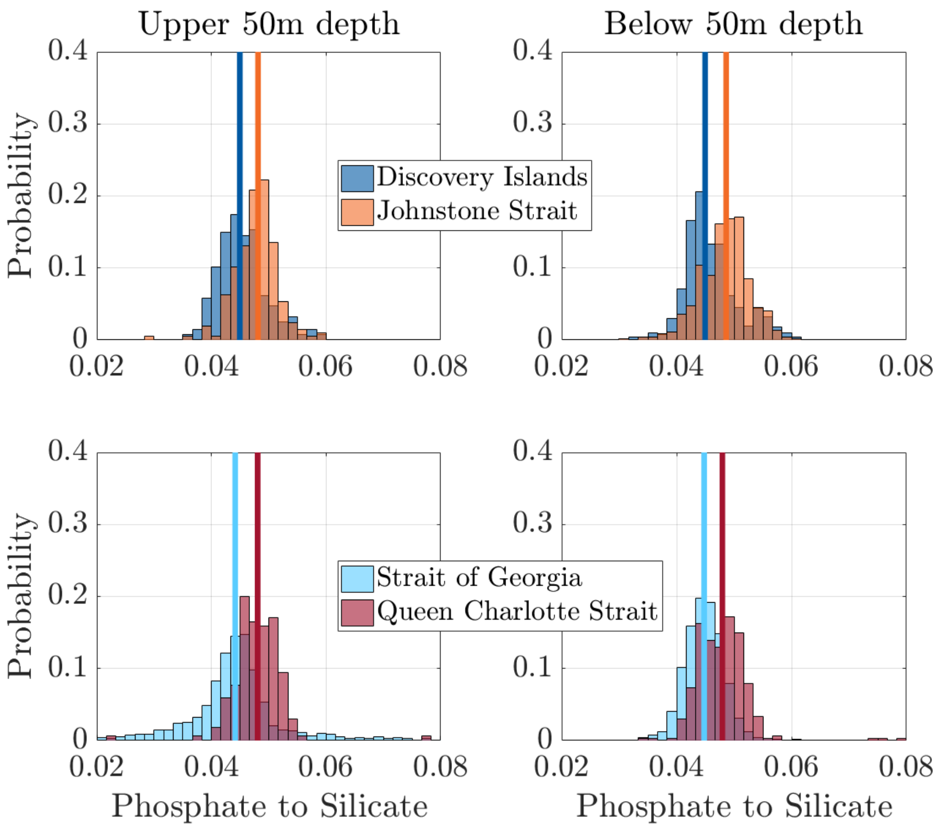

Figure 8. As in Figure 6, but for the molar ratio of phosphate to silicate.

to silicate ratio has the smallest regional variation (P:Si, Figure 8), with a 7% difference in median value between 0.048 in QCSt/JS and 0.045 in the SoG/DI (Table 1). Distributions of all three nutrient molar ratios in QCSt and JS are statistically distinct from those in the SoG and DI at the 99% confidence interval ($p<0.001$ for all three ratios) based on a Kolmogorov-Smirnov test, in both the upper and lower water column.

Nutrient ratios vary regionally as a result of relative differences in nutrient concentration (Table 1, Supporting Information S.3). Median nutrient concentrations are lowest in QCSt and highest in the SoG, with relatively high silicate concentrations in the SoG contributing significantly to regional differences. Nutrient ratio distributions in the upper water column in the SoG have long tails (Figures 6, 7, 8), evidence of occasional nitrate and/or phosphate depletion (Masson & Peña, 2009), which is common in coastal waters particularly in the late summer (Howarth & Marino, 2006). However, nutrient concentrations in all regions are rarely limiting (Table 1, Supporting Information S.3). In addition to differing degrees of nutrient depletion by biology, other possible causes for the regional differences in nutrient ratios are differences in source waters or transport pathways for nutrient input, as discussed further in Section 4.2.

3.5 Seasonal upwelling

Closer examination of the seasonal cycle of physical water properties and nutrient ratios in the deep waters of QCSt and the SoG reveals differences in the timing and magnitude of upwelled water arriving from the Northeast Pacific Ocean. (Seasonal variations in deep water properties in JS and the DI are suppressed due to tidal mixing, but are otherwise qualitatively similar to those in QCSt and the SoG respectively.) In the lower water column in QCSt, water upwelled from the deep Northeast Pacific causes decreased temperatures (Figure 4d), increased salinity (Figure 4b), increased density (Figure 9a), and increased nutrient concentrations (Figure 9b) beginning in April and peaking in August. By contrast, upwelled water in the SoG region is associated with only minor variations in the seasonal cycle of these properties, likely due to significant modification in Haro Strait before its arrival in the northern Strait of Georgia (LeBlond et al., 1991; Mackas & Harrison, 1997). Here, a small seasonal increase in deep salinity (Figure 4b) and density (Figure 9a) reaches a maximum in October/November, with no accompanying increase in nutrient concentration or decrease in temperature (these attain their maximum and minimum values, respectively, in July). These differences in seasonal cycle magni-

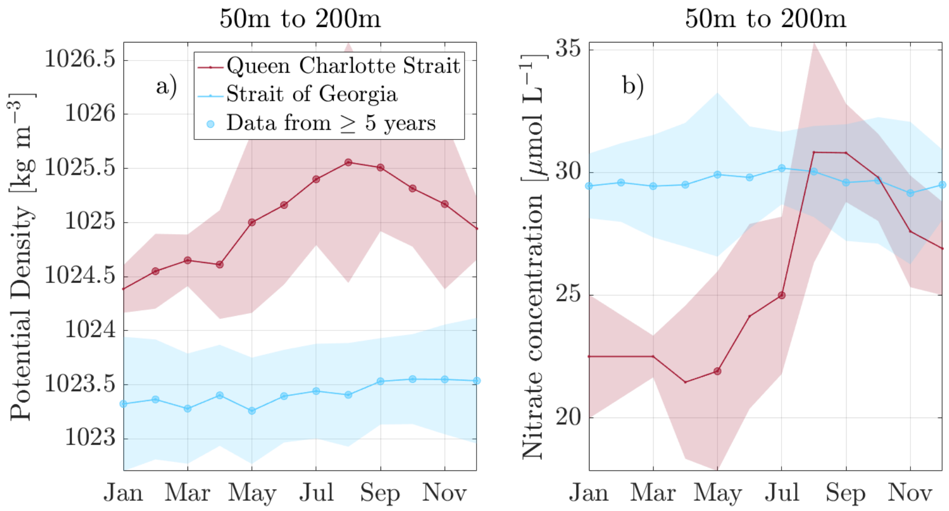

Figure 9. a) Potential density and b) nitrate concentration by month for the lower water column (50-200 m) in Queen Charlotte Strait (red) and the Strait of Georgia (light blue). Lines give the monthly median density and nitrate values, with large dots indicating at data from at least five years. Shading gives the 25-75% interquartile range.

tude and the timing of the arrival of upwelled water in QCSt/JS vs. the SoG/DI regions are significant because they suggest distinct transport pathways for upwelled water (we suggest these pathways are to the north of Vancouver Island for QCSt/JS and to the south through the Strait of Juan de Fuca for the SoG/DI), with little to no exchange of deep water through the tidal mixing frontal zone. These differences in the seasonality of deep water properties between regions adds further support to the emerging picture of QCSt/JS and the SoG/DI as separate environments, largely isolated from each other, and likely to respond differently to changes in large-scale open-ocean forcing.

4 Discussion

The observed regional differences in physical and biogeochemical properties reported herein are consistent with an effective disruption of the two-layer estuarine exchange flow between QCSt and the SoG due to tidal mixing. Here we address, first, possible implications for circulation, and second, some direct and indirect effects on marine ecosystems in the study area.

4.1 Tidal mixing and circulation

A visualization of the average density structure along a transect connecting eastern QCSt to the northern SoG during upwelling favorable conditions (Figure 10) shows a strong lateral density gradient between JS and the DI. The abrupt transition between these regions in the tidal mixing frontal zone is visible as near-vertical isopycnal structure, indicating homogenization of the water column, for a narrow range of densities around 1023 kg m^{-3} (Figure 10; ~200 km). As demonstrated in Section 3.3, waters in JS are almost completely separate in density space from waters in the DI at all depths below the near-surface (<10 m). Only very near the surface do we see evidence of freshwater advection from the DI into JS, a signal which is likely caused by wind forcing dominating the direction of surface currents there (Chandler et al., 2017). Although the scarcity of data in the tidal mixing frontal zone precludes identifying the exact number and location of individual density fronts, we estimate that the lateral gradient between regions spans a distance of at least ~75 km within the narrow, shallow channels of JS and the DI (Figure 10; ~150-225 km). Vigorous tidal mixing has been reported both within the tidal mixing frontal zone and in adjacent channels; Thomson1981 mentions particularly strong tidal mixing over the Discovery Passage sill (Figure 10; ~275 km). The relatively shallow sills between regions also affect the density structure in the study area. The densest waters in QCSt are isolated from JS by the <100 m deep sill at ~100 km along the transect. Similarly, the <100 m deep Discovery Passage sill prevents dense deep waters in the SoG from entering the DI. In combination, these factors produce the dramatic lateral density gradient between the QCSt/JS and SoG/DI regions.

Although details of the circulation within our study area are not well-known, the abrupt and persistent transition in density and other water properties that we document is consistent with limited exchange between the QCSt/JS and SoG/DI regions in all subsurface waters (i.e. >10 m). Rather than the strong two-layer estuarine exchange flow typical of stratified estuaries, transport through the tidal mixing frontal zone is likely to occur via a weak residual one-way flow from the DI towards JS, similar to that observed in a well-mixed estuary (e.g. MacCready & Geyer, 2010). In such a case where the horizontal advection is reduced, the primary transport of properties through the tidal mixing frontal zone must occur via mixing, operating more slowly over smaller spatial scales (MacCready et al., 2018). The inhibition of horizontal transport is additionally expected to cause recirculation of much of the inflowing water (Griffin & LeBlond, 1990;

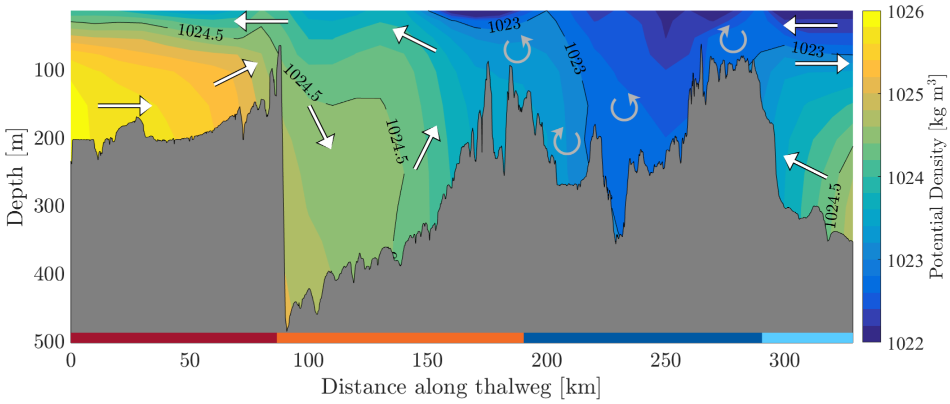

Figure 10. Lateral transect of potential density following the thalweg (line of deepest bathymetry) from QCSt to the SoG during mid-summer (June to August) using data from all available years. Data are binned every 10 km in the horizontal, and every 25 m in the vertical to 100 m depth, then every 50 m to 500 m depth (due to a paucity of full-depth profiles). Black contours show select isopycnals as indicated. Coloured bars along the x-axis give the boundaries of the four regions as shown in Figure 1. Data in the very near-surface waters (<10 m depth) have been excluded. White arrows show the hypothesized recirculation and transport pathways of inflowing water from QCSt into JS and from the SoG into the DI respectively. Gray arrows indicate the region of strong mixing in the tidal mixing frontal zone and Discovery Passage.

Hibiya & LeBlond, 1993; Park & Kuo, 1996; MacCready, 1999). Based on these considerations, we propose a hypothetical circulation pattern consistent with our results and past studies of circulation in the study area. This circulation is illustrated schematically for upwelling favorable conditions in Figure 10. Below the very near-surface, our results suggest that a significant fraction of the water entering JS from QCSt is recirculated back out to QCSt. Similarly our results suggest that a significant proportion of water entering the DI from the SoG is recirculated back to the SoG. While the visualization in Figure 10 is specific to the months of June to August, our results demonstrate that the transition in properties across the tidal mixing frontal zone persists year-round (Section 3.2), suggesting that these recirculations driven by tidal mixing occur regardless of season.

We further suggest likely transport pathways for the inflowing water on either side of the tidal mixing frontal zone (Figure 10). We hypothesize that during summer dense upwelled water flows from QCSt over the sill into the deep JS basin, is mixed vertically within the tidal mixing frontal zone, and passes back out to QCSt near the surface. This circulation in JS is similar to that in other deep basins situated between shallow sills, such as the main basin in nearby Puget Sound (Ebbesmeyer & Barnes, 1980), and shares similarities with partially-mixed (moderately-stratified) estuaries (MacCready & Geyer, 2010) with fresh water from the DI playing the role of river inflow at the head of the estuary. On the other side of the tidal mixing frontal zone, we hypothesize that water from the SoG enters Discovery Passage in the DI primarily above ∼100 m depth, is mixed vertically with denser water intermittently sourced from the SoG, and passes back out to the SoG at mid-depth (>100 m on average, Thomson (1981)). These proposed transport pathways are consistent with the similarity in water properties observed between JS and the upper 30-50 m of QCSt (<1025 kg m^{-3}), the similarity in properties observed between the SoG and DI in the upper ∼80 m (<1023 kg m^{-3}), the predictions of regional models (Foreman et al., 2006, 2012; Khangaonkar et al., 2017; Olson et al., 2020), and current meter records in JS (Thomson & Huggett, 1980) and Discovery Passage (Foreman et al., 2012).

Although it is not surprising that QCSt and the SoG have different water properties, as the latter is an inland sea while the former opens directly to the continental shelf and Northeast Pacific Ocean, conventional wisdom has held that waters from the SoG are advected through the DI and JS into QCSt and vice-versa (e.g. Godin et al., 1981) driving a significant exchange of properties. Our results and hypothesized circulation suggest that a more accurate view of the QCSt/JS and SoG/DI regions are as distinct, largely isolated marine environments, with different physical water properties, seasonality, connectivity to the open ocean, and pathways of nutrient delivery. An important implication of this is that we expect regional responses to stressors to differ, particularly for stressors originating in the open ocean.

As an example of differing regional responses to a stressor, we briefly examine the effect of the marine heatwave known as The Blob on temperatures in the QCSt/JS and SoG/DI regions (Figure 11). This heatwave and a subsequent El Niño impinged on BC coastal waters beginning in 2014 (Bond et al., 2015), with a subsurface expression affecting coastal waters through at least 2018 (Jackson et al., 2018). We compare distributions of temperature in the upper water column pre-2014 vs. during the Blob years in the QCSt/JS vs. SoG/DI regions. The anomalous heat associated with this heatwave is visible on both sides of the tidal mixing frontal zone, however the effects of the heatwave are more pronounced in QCSt/JS, presumably due to its higher connectivity with the open ocean. In particular, the temperature anomaly associated with the heatwave is larger in QCSt/JS; the median of the temperature distribution shifts upward by 0.81°C (compared to 0.66°C in the SoG/DI). In addition, there is a complete loss of the coldest waters in QCSt/JS, which is not observed on the SoG/DI side of the tidal mixing frontal zone. In contrast, the SoG/DI region experiences little change in the range of temperatures observed, though cold temperatures become more rare and warm temperatures more common.

4.2 Implications for ecosystems

Tidal mixing has important direct and indirect implications for ecosystems. First, we consider the direct role of tidal mixing in vertical nutrient transport and light availability. Our results show the arrival of upwelled water in JS in summer (Figure 4), and we hypothesize that strong tidal mixing and recirculation (Figure 10) acts to bring deep nutrients to the surface, which then exit into the more strongly-stratified waters of QCSt. On the other side of the tidal mixing frontal zone, these dynamics result in nutrient-rich water re-entering the SoG at mid-depth in the Discovery Passage plume (e.g. Olson et al., 2020) and help fuel phytoplankton blooms in the SoG (Del Bel Belluz et al., 2020). Despite high near-surface nutrient concentrations (Table 1), the weakly-stratified waters of JS and the DI are themselves regions of low primary productivity (Mahara et al., 2020).

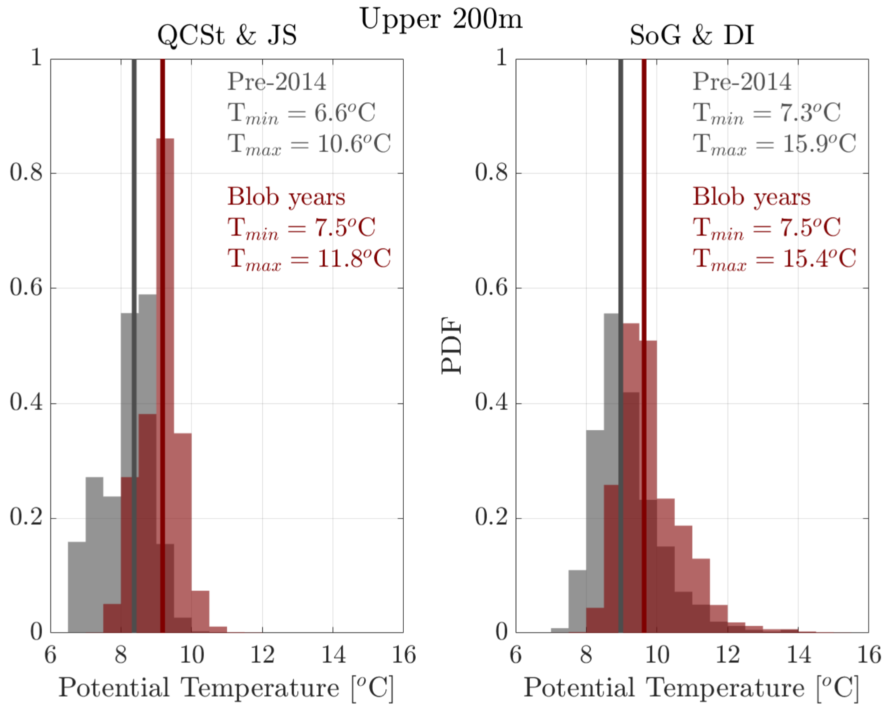

Figure 11. Distributions of potential temperature from 10-200 m depth for years when the marine heatwave known as The Blob affected coastal waters (dark red) and for years prior to this event (gray) in QCSt/JS (left) and in the SoG/DI (right). Vertical lines give the median of each distribution. Data used are binned every 25 m in the vertical. Data from Jan-Mar are excluded as no samples are available in QCSt during those months for 2014-onwards. Minimum and maximum temperatures for the two periods are as given.

These high-nutrient, low-productivity conditions are attributed to full-depth tidal mixing limiting the light available to phytoplankton for growth (Masson & Peña, 2009; McKinnell et al., 2014; Murray et al., 2015). The resulting low primary productivity is known to have wider ecosystem effects, with migrating juvenile salmon experiencing poor foraging success in JS and the DI (James et al., 2020). However, our results suggest that while tidal mixing in JS and the DI limits productivity within those regions, it may simultaneously enhance and sustain the overall high levels of productivity observed in QCSt and the SoG.

An important implication of the differing transport pathways resulting from the recirculation of inflowing water caused by tidal mixing is that the primary sources of nutrient-rich waters supplying QCSt and the SoG likely differ. This may explain the observed regional differences in nutrient molar ratios (Figures 6, 7, 8). Seasonal upwelling appears to be the dominant source of nutrient replenishment in QCSt/JS, with upwelled water arriving from the open ocean via Queen Charlotte Sound. Consistent with this picture, nutrient ratios in QCSt/JS are closer to ideal Redfield-Brzezinski values, which describe ratios typical of open-ocean conditions (Brzezinski, 1985). By contrast, nutrient ratios in the SoG/DI are further from these ideal values, as expected for coastal waters with major inputs of silicate from freshwater runoff (Whitney et al., 2005) and accumulation of nutrients through remineralization in SoG waters with high residence time (Pawlowicz et al., 2007; Sutton et al., 2013). As such, while nutrient cycling in QCSt/JS is likely to be directly impacted by changes in the volume or properties of upwelled water, the SoG/DI region is likely more susceptible to changes in terrestrial and river inputs or in-situ water properties that affect remineralization in the water column and sediments.

Differences in oceanic nutrient ratios provide more than a measure of nutrient limitation; regional differences in nutrient ratios are expected to influence the species composition of phytoplankton communities and their cellular stoichiometry (Geider & La Roche, 2002; Arrigo, 2005; Klausmeier et al., 2008). Although nutrients are typically plentiful across the study area (Section 3.4, Supporting Information S.3), nutrient molar ratios have the potential to limit the productivity of some phytoplankton species. For example, in QCSt where ratios are most similar to open-ocean values, we might expect phytoplankton communities to share similarities with nearby open-ocean or continental shelf communities. In the SoG, where ratios are further from the ideal Redfield-Brzezinski values, we might expect significant differences in species composition. This is an area of active research, and indeed, cross-shelf differences in phytoplankton community composition and size structure in response to changing nutrient ratios have been demonstrated in Alaska (Strom et al., 2006). Phytoplankton species composition and prevalence can in turn affect the quantity and nutritional quality of their zooplankton grazers (El-Sabaawi et al., 2009; Costalago et al., 2020), with implications for the next trophic level, including juvenile salmon and forage fish (e.g. Pacific herring) (Litzow et al., 2006; Godefroid et al., 2019; James et al., 2020). The tidal mixing and its hypothesized effects on circulation therefore impact not only levels of primary productivity via nutrient transport, but also potentially underlie certain regional ecosystem differences within the study area.

5 Summary

Using a combined DFO, UBC, and Hakai Institute data product, we document a spatially-abrupt and temporally-persistent transition in physical water properties and nutrient ratios bisecting our study area in British Columbia coastal waters. The transition occurs in the weakly-stratified channels of the eastern Discovery Islands and Johnstone Strait, between Queen Charlotte Strait and the Strait of Georgia, where strong tidal mixing appears to disrupt the two-layer estuarine exchange flow and drive recirculations of inflowing water. We quantify an abrupt change in salinity and temperature across this 'tidal mixing frontal zone', with properties in Queen Charlotte Strait and Johnstone Strait more closely resembling cool and saline open-ocean conditions in all seasons and more strongly influenced by the summer arrival of dense, cold, nutrient-rich water upwelled from the Northeast Pacific Ocean. We identify a dramatic lateral gradient in density, previously described by Thomson (1976, 1981), and show that it spans the full depth of the water column and persists year-round for the duration of the multi-decadal data record. We find that distributions of nutrient molar ratios in Queen Charlotte Strait and Johnstone Strait are statistically distinct from those in the northern Strait of Georgia and Discovery Islands, and are closer to ideal open-ocean Redfield-Brzezinski values.

The 'tidal mixing frontal zone' provides an ideal case study for the ability of strong, sustained tidal mixing to maintain regional differences in water properties. Despite lacking direct measurements of circulation, our results suggest limited exchange of water through the region of strongest tidal mixing. As such, Queen Charlotte Strait and the Strait of Georgia appear largely isolated from each other and are shown to respond differently to environmental stressors such as marine heatwaves. Furthermore, significant regional differences in marine environmental conditions and nutrient transport pathways, such as those observed within the study area, are expected to influence both the quantity and quality of primary production available to higher trophic levels. Our results demonstrate the degree to which tidal mixing can result in such regionalization, and may be broadly relevant to other highly productive coastal habitats such as those found in Alaska and on the southwest coasts of Chile, New Zealand, and Scandinavia.

Acknowledgments

Data collected by DFO and UBC and used in this study are archived and publicly available at cioospacific.ca and at waterproperties.ca. The data collected by DFO are also accessible through the Institute of Ocean Sciences Data Archive, Ocean Sciences Division, Department of Fisheries and Oceans Canada at www.pac.dfo-mpo.gc.ca/science/oceans/data-donnees/index-eng.html. Data collected by the Hakai Institute are available at hecate.hakai.org. We thank the many scientists, students, technicians, and crew from the Pacific Biological Station, the Institution of Ocean Sciences, the University of British Columbia, and the Hakai Institute whose collective efforts to sample and understand the BC coastal ocean over the last 90 years have provided us with the observations and past research that made this work possible. We are particularly grateful for the efforts of Rick Thomson who pioneered much of the research in the Johnstone Strait region. We also specifically acknowledge the field crews at the Hakai Institute's Quadra Island field station and Salmon Coast Field Station for their time and energy in the field collection and curation of oceanographic data.

This research was conducted as part of the Hakai Institute's Juvenile Salmon Program, funded by the Tula Foundation. H. Dosser received funding from the Tula-Mitacs Canada Grants IT09911 through internships No. FR23012, FR23020, and FR23028 and through a Marine Environmental Observation, Prediction and Response Network (MEOPAR) - Networks of Centres of Excellence (NCE) Postdoctoral Fellowship Award. B. Hunt and J. Jackson were funded by the Tula Foundation. S.Waterman was supported by MEOPAR - NCE and Ocean Networks Canada through Early Career Faculty Grant 2-02-03-061.1 and the Natural Sciences and Engineering Research Council of Canada (NSERC) through Discovery Grants Program Award RGPIN-2020-05799.

References

Arimitsu, M., Piatt, J., & Mueter, F. (2016). Influence of glacier runoff on ecosystem structure in Gulf of Alaska fjords. *Mar. Ecol. Prog. Ser.*, *560*, 19–40. Retrieved from http://www.int-res.com/abstracts/meps/v560/p19-40/ doi: 10.3354/meps11888

Arrigo, K. R. (2005). Marine microorganisms and global nutrient cycles. *Nature*, *437*(7057), 349–355. Retrieved from http://www.nature.com/articles/nature04159 doi: 10.1038/nature04159

Bond, N. A., Cronin, M. F., Freeland, H., & Mantua, N. (2015). Causes and impacts of the 2014 warm anomaly in the NE Pacific. *Geophys. Res. Lett.*, *42*(9), 3414–3420. Retrieved from http://doi.wiley.com/10.1002/2015GL063306 doi: 10.1002/2015GL063306

Brzezinski, M. A. (1985). The Si:C:N ratio of marine diatoms: interspecific variability and the effect of some environmental variables. *Journal of Phycology*, *21*(3), 347–357. Retrieved from http://doi.wiley.com/10.1111/j.0022-3646.1985.00347.x doi: 10.1111/j.0022-3646.1985.00347.x

Canadian Tide and Current Tables / Tables des marées et courants du Canada. (2019). The Canadian Hydrographic Service, Fisheries and Oceans Canada. Retrieved from www.charts.gc.ca

Chandler, P., Foreman, M. G., Ouellet, M., Mimeault, C., & Wade, J. (2017). *Oceanographic and environmental conditions in the Discovery Islands, British Columbia* (DFO Can. Sci. Advis. Sec. Res. Doc. 2017/071, viii + 51).

Costalago, D., Forster, I., Nemcek, N., Neville, C., Perry, R. I., Young, K., & Hunt, B. P. V. (2020). Seasonal and spatial dynamics of the planktonic trophic biomarkers in the Strait of Georgia (northeast Pacific) and implications for fish. *Sci Rep*, *10*(1), 8517. Retrieved from http://www.nature.com/articles/s41598-020-65557-1 doi: 10.1038/s41598-020-65557-1

Crawford, W. R., & Peña, M. A. (2013). Declining Oxygen on the British Columbia Continental Shelf. *Atmosphere-Ocean*, *51*(1), 88–103. Retrieved from https://www.tandfonline.com/doi/full/10.1080/07055900.2012.753028 doi: 10.1080/07055900.2012.753028

Del Bel Belluz, J., Peña, M., Jackson, J., & Nemcek, M. (2020). Phytoplankton composition and environmental drivers in the northern Strait of Georgia (Salish Sea), British Columbia, Canada. *Estuaries Coast*.

Di Lorenzo, E., & Mantua, N. (2016). Multi-year persistence of the 2014/15 North Pacific marine heatwave. *Nature Clim Change*, *6*(11), 1042–1047. Retrieved from http://www.nature.com/articles/nclimate3082 doi: 10.1038/nclimate3082

Ebbesmeyer, C. C., & Barnes, C. A. (1980). Control of a fjord basin's dynamics by tidal mixing in embracing sill zones. *Estuarine and Coastal Marine Science*, *11*(3), 311–330. Retrieved from https://linkinghub.elsevier.com/retrieve/pii/S0302352480800867 doi: 10.1016/S0302-3524(80)80086-7

El-Sabaawi, R., Dower, J. F., Kainz, M., & Mazumder, A. (2009). Characterizing dietary variability and trophic positions of coastal calanoid copepods: insight from stable isotopes and fatty acids. *Mar Biol*, *156*(3), 225–237. Retrieved from http://link.springer.com/10.1007/s00227-008-1073-1 doi: 10.1007/s00227-008-1073-1

Evans, W., Pocock, K., Hare, A., Weekes, C., Hales, B., Jackson, J., … Feely, R. A. (2019). Marine CO2 Patterns in the Northern Salish Sea. *Front. Mar. Sci.*, *5*, 536. Retrieved from https://www.frontiersin.org/article/10.3389/fmars.2018.00536/full doi: 10.3389/fmars.2018.00536

Feely, R. A., Alin, S. R., Carter, B., Bednaršek, N., Hales, B., Chan, F., … Juranek, L. (2016). Chemical and biological impacts of ocean acidification along the west coast of North America. *Estuarine, Coastal and Shelf Science*, *183*, 260–270. Retrieved from https://linkinghub.elsevier.com/retrieve/pii/S0272771416302980 doi: 10.1016/j.ecss.2016.08.043

Foreman, M., Stucchi, D., Zhang, Y., & Baptiste, A. (2006). Estuarine and Tidal Currents in the Broughton Archipelago. *Atmosphere-Ocean*, *44*(1), 47–63. Retrieved from https://www.tandfonline.com/doi/full/10.3137/ao.440104 doi: 10.3137/ao.440104

Foreman, M., Stucchi, D. J., Garver, K. A., Tuele, D., Isaac, J., Grime, T., … Morrison, J. (2012). A Circulation Model for the Discovery Islands, British Columbia. *Atmosphere-Ocean*, *50*(3), 301–316. Retrieved from http://www.tandfonline.com/doi/abs/10.1080/07055900.2012.686900 doi: 10.1080/07055900.2012.686900

Foreman, M., Sutherland, G., & Cummins, P. (2004). M2 tidal dissipation around Vancouver Island: an inverse approach. *Continental Shelf Research*, *24*(18), 2167–2185. Retrieved from https://linkinghub.elsevier.com/retrieve/pii/S0278434304001700 doi: 10.1016/j.csr.2004.07.008

Gay, S. M., & Vaughan, S. L. (2001). Seasonal hydrography and tidal currents of bays and fjords in Prince William Sound, Alaska: Physical oceanography of nursery habitats of juvenile Pacific herring. *Fisheries Oceanography*, *10*, 159–193. Retrieved from http://doi.wiley.com/10.1046/j.1054-6006.2001.00041.x doi: 10.1046/j.1054-6006.2001.00041.x

Geider, R., & La Roche, J. (2002). Redfield revisited: variability of C:N:P in marine microalgae and its biochemical basis. *European Journal of Phycology*, *37*(1), 1–17. Retrieved from http://www.tandfonline.com/doi/abs/10.1017/S0967026201003456 doi: 10.1017/S0967026201003456

Godefroid, M., Boldt, J. L., Thorson, J. T., Forrest, R., Gauthier, S., Flostrand, L., … Galbraith, M. (2019). Spatio-temporal models provide new insights on the biotic and abiotic drivers shaping Pacific Herring (Clupea pallasi) distribution. *Progress in Oceanography*, *178*, 102198. Retrieved from https://linkinghub.elsevier.com/retrieve/pii/S0079661119300850 doi: 10.1016/j.pocean.2019.102198

Godin, G., Candela, J., & de la Paz-Vela, R. (1981). On the feasibility of detecting net transports in and out of Georgia strait with an array of current meters. *Atmosphere-Ocean*, *19*(2), 148–157. Retrieved from http://www.tandfonline.com/doi/abs/10.1080/07055900.1981.9649106 doi: 10.1080/07055900.1981.9649106

Griffin, D. A., & LeBlond, P. H. (1990). Estuary/ocean exchange controlled by spring-neap tidal mixing. *Estuarine, Coastal and Shelf Science*, *30*(3), 275–297. Retrieved from https://linkinghub.elsevier.com/retrieve/pii/027277149090052S doi: 10.1016/0272-7714(90)90052-S

Harrison, P. J., Fulton, J. D., Taylor, F. J. R., & Parsons, T. R. (1983). Review of the Biological Oceanography of the Strait of Georgia: Pelagic Environment. *Can. J. Fish. Aquat. Sci.*, *40*(7), 1064–1094. Retrieved from http://www.nrcresearchpress.com/doi/10.1139/f83-129 doi: 10.1139/f83-129

Hibiya, T., & LeBlond, P. H. (1993). The Control of Fjord Circulation by Fortnightly Modulation of Tidal Mixing Processes. *Journal of Physical Oceanography*, *23*(9), 2042–2052. Retrieved from `https://doi.org/10.1175/1520-0485(1993)023<2042:TCOFCB>2.0.CO;2` doi: 10.1175/1520-0485(1993)023⟨2042:TCOFCB⟩2.0.CO;2

Howarth, R. W., & Marino, R. (2006). Nitrogen as the limiting nutrient for eutrophication in coastal marine ecosystems: Evolving views over three decades. *Limnol. Oceanogr.*, *51*(1 part 2), 364–376. Retrieved from `https://onlinelibrary.wiley.com/doi/abs/10.4319/lo.2006.51.1_part_2.0364` doi: 10.4319/lo.2006.51.1_part_2.0364

Institute of Ocean Sciences Data Archive. (2020). Ocean Sciences Division, Department of Fisheries and Oceans Canada. Retrieved 2018-07-30, from `http://www.pac.dfo-mpo.gc.ca/science/oceans/data-donnees/index-eng.html`

Iriarte, J. L., Pantoja, S., & Daneri, G. (2014). Oceanographic Processes in Chilean Fjords of Patagonia: From small to large-scale studies. *Progress in Oceanography*, *129*, 1–7. Retrieved from `https://linkinghub.elsevier.com/retrieve/pii/S0079661114001670` doi: 10.1016/j.pocean.2014.10.004

Jackson, J. M., Johnson, G. C., Dosser, H. V., & Ross, T. (2018). Warming From Recent Marine Heatwave Lingers in Deep British Columbia Fjord. *Geophys. Res. Lett.*, *45*(18), 9757–9764. Retrieved from `http://doi.wiley.com/10.1029/2018GL078971` doi: 10.1029/2018GL078971

James, S. E., Pakhomov, E. A., Mahara, N., & Hunt, B. P. V. (2020). Running the trophic gauntlet: Empirical support for reduced foraging success in juvenile salmon in tidally mixed coastal waters. *Fish Oceanogr*, *29*(3), 290–295. Retrieved from `https://onlinelibrary.wiley.com/doi/abs/10.1111/fog.12471` doi: 10.1111/fog.12471

Johannessen, S. C., Masson, D., & Macdonald, R. W. (2014). Oxygen in the deep Strait of Georgia, 1951-2009: The roles of mixing, deep-water renewal, and remineralization of organic carbon. *Limnol. Oceanogr.*, *59*(1), 211–222. Retrieved from `http://doi.wiley.com/10.4319/lo.2014.59.1.0211` doi: 10.4319/lo.2014.59.1.0211

Khangaonkar, T., Long, W., & Xu, W. (2017). Assessment of circulation and inter-basin transport in the Salish Sea including Johnstone Strait and Discovery Islands pathways. *Ocean Modelling*, *109*, 11–32. Retrieved from https://linkinghub.elsevier.com/retrieve/pii/S1463500316301408 doi: 10.1016/j.ocemod.2016.11.004

Klausmeier, C. A., Litchman, E., Daufresne, T., & Levin, S. A. (2008). Phytoplankton stoichiometry. *Ecol Res*, *23*(3), 479–485. Retrieved from http://doi.wiley.com/10.1007/s11284-008-0470-8 doi: 10.1007/s11284-008-0470-8

Kolmogorov–Smirnov Test. (2008). In *The Concise Encyclopedia of Statistics* (pp. 283–287). New York, NY: Springer New York. Retrieved from http://link.springer.com/10.1007/978-0-387-32833-1_214 doi: 10.1007/978-0-387-32833-1_214

LeBlond, P. H. (1983). The Strait of Georgia: functional anatomy of a coastal sea. *Can. J. Fish. Aquat. Sci.*, *40*(7), 1033–1063. Retrieved from http://www.nrcresearchpress.com/doi/10.1139/f83-128 doi: 10.1139/f83-128

LeBlond, P. H., Ma, H., Doherty, F., & Pond, S. (1991). Deep and intermediate water replacement in the Strait of Georgia. *Atmosphere-Ocean*, *29*(2), 288–312. Retrieved from http://www.tandfonline.com/doi/abs/10.1080/07055900.1991.9649406 doi: 10.1080/07055900.1991.9649406

Litzow, M., Bailey, K., Prahl, F., & Heintz, R. (2006). Climate regime shifts and reorganization of fish communities: the essential fatty acid limitation hypothesis. *Mar. Ecol. Prog. Ser.*, *315*, 1–11. Retrieved from http://www.int-res.com/abstracts/meps/v315/p1-11/ doi: 10.3354/meps315001

Loder, J. W., Drinkwater, K. F., Oakey, N. S., & Horne, E. P. W. (1994). Circulation, hydrographic structure and mixing at tidal fronts: the view from Georges Bank. In H. Charnock, K. R. Dyer, J. M. Huthnance, P. S. Liss, J. H. Simpson, & P. B. Tett (Eds.), *Understanding the North Sea System* (pp. 69–82). Dordrecht: Springer Netherlands. Retrieved from http://link.springer.com/10.1007/978-94-011-1236-9_6 doi: 10.1007/978-94-011-1236-9_6

MacCready, P. (1999). Estuarine Adjustment to Changes in River Flow and Tidal Mixing. *Journal of Physical Oceanography*, *29*(4), 708–726. Retrieved from https://doi.org/10.1175/1520-0485(1999)029<0708:EATCIR>2.0.CO;2 doi: 10.1175/1520-0485(1999)029⟨0708:EATCIR⟩2.0.CO;2

MacCready, P., & Geyer, W. R. (2010). Advances in Estuarine Physics. *Annu. Rev. Mar. Sci.*, *2*(1), 35–58. Retrieved from `http://www.annualreviews.org/doi/10.1146/annurev-marine-120308-081015` doi: 10.1146/annurev-marine-120308-081015

MacCready, P., Geyer, W. R., & Burchard, H. (2018). Estuarine Exchange Flow Is Related to Mixing through the Salinity Variance Budget. *Journal of Physical Oceanography*, *48*(6), 1375–1384. Retrieved from `https://journals.ametsoc.org/jpo/article/48/6/1375/42551/Estuarine-Exchange-Flow-Is-Related-to-Mixing` doi: 10.1175/JPO-D-17-0266.1

Mackas, D. L., & Harrison, P. J. (1997). Nitrogenous Nutrient Sources and Sinks in the Juan de Fuca Strait/Strait of Georgia/Puget Sound Estuarine System: Assessing the Potential for Eutrophication. *Estuarine, Coastal and Shelf Science*, *44*(1), 1–21. Retrieved from `https://linkinghub.elsevier.com/retrieve/pii/S0272771496901109` doi: 10.1006/ecss.1996.0110

Mahara, N., Pakhomov, E. A., Dosser, H. V., & Hunt, B. P. V. (2020). How zooplankton communities are shaped in a complex and dynamic coastal system with strong tidal influence. *Estuarine, Coastal and Shelf Science*. doi: 10.1016/j.ecss.2020.107103

Masson, D. (2002). Deep Water Renewal in the Strait of Georgia. *Estuarine, Coastal and Shelf Science*, *54*(1), 115–126. Retrieved from `https://linkinghub.elsevier.com/retrieve/pii/S0272771401908339` doi: 10.1006/ecss.2001.0833

Masson, D., & Cummins, P. F. (2004). Observations and modeling of seasonal variability in the Straits of Georgia and Juan de Fuca. *J Mar Res*, *62*(4), 491–516. Retrieved from `http://www.ingentaselect.com/rpsv/cgi-bin/cgi?ini=xref&body=linker&reqdoi=10.1357/0022240041850075` doi: 10.1357/0022240041850075

Masson, D., & Peña, A. (2009). Chlorophyll distribution in a temperate estuary: The Strait of Georgia and Juan de Fuca Strait. *Estuarine, Coastal and Shelf Science*, *82*(1), 19–28. Retrieved from `https://linkinghub.elsevier.com/retrieve/pii/S027277140900002X` doi: 10.1016/j.ecss.2008.12.022

McKinnell, S., Curchitser, E., Groot, K., Kaeriyama, M., & Trudel, M. (2014). Oceanic and atmospheric extremes motivate a new hypothesis for variable marine survival of Fraser River sockeye salmon. *Fish. Oceanogr.*, *23*(4), 322–341. Retrieved from http://doi.wiley.com/10.1111/fog.12063 doi: 10.1111/fog.12063

Murray, J. W., Roberts, E., Howard, E., O'Donnell, M., Bantam, C., Carrington, E., ... Fay, A. (2015). An inland sea high nitrate-low chlorophyll (HNLC) region with naturally high pCO $_2$. *Limnol. Oceanogr.*, *60*(3), 957–966. Retrieved from https://onlinelibrary.wiley.com/doi/10.1002/lno.10062 doi: 10.1002/lno.10062

Olson, E. M., Allen, S. E., Do, V., Dunphy, M., & Ianson, D. (2020). Assessment of Nutrient Supply by a Tidal Jet in the Northern Strait of Georgia Based on a Biogeochemical Model. *J. Geophys. Res. Oceans*, *125*(8). Retrieved from https://onlinelibrary.wiley.com/doi/10.1029/2019JC015766 doi: 10.1029/2019JC015766

Park, K., & Kuo, A. Y. (1996). Effect of variation in vertical mixing on residual circulation in narrow, weakly nonlinear estuaries. In D. G. Aubrey & C. T. Friedrichs (Eds.), *Coastal and Estuarine Studies* (Vol. 53, pp. 301–317). Washington, D. C.: American Geophysical Union. Retrieved from http://www.agu.org/books/ce/v053/CE053p0301/CE053p0301.shtml doi: 10.1029/CE053p0301

Pawlowicz, R., Riche, O., & Halverson, M. (2007). The circulation and residence time of the strait of Georgia using a simple mixing-box approach. *Atmosphere-Ocean*, *45*(4), 173–193. Retrieved from http://www.tandfonline.com/doi/abs/10.3137/ao.450401 doi: 10.3137/ao.450401

Riche, O., Johannessen, S., & Macdonald, R. (2014). Why timing matters in a coastal sea: Trends, variability and tipping points in the Strait of Georgia, Canada. *Journal of Marine Systems*, *131*, 36–53. Retrieved from https://linkinghub.elsevier.com/retrieve/pii/S092479631300225X doi: 10.1016/j.jmarsys.2013.11.003

Smethie, W. M. (1987). Nutrient regeneration and denitrification in low oxygen fjords. *Deep Sea Research Part A. Oceanographic Research Papers*, *34*(5-6), 983–1006. Retrieved from https://linkinghub.elsevier.com/retrieve/pii/0198014987900495 doi: 10.1016/0198-0149(87)90049-5

Stanton, B. R., & Pickard, G. L. (1980). Physical Oceanography of the New Zealand Fjords. In H. J. Freeland, D. M. Farmer, & C. D. Levings (Eds.), *Fjord Oceanography* (pp. 329–332). Boston, MA: Springer US. Retrieved from `http://link.springer.com/10.1007/978-1-4613-3105-6_26` doi: 10.1007/978-1-4613-3105-6_26

Strom, S., Olson, M., Macri, E., & Mord, C. (2006). Cross-shelf gradients in phytoplankton community structure, nutrient utilization, and growth rate in the coastal Gulf of Alaska. *Mar. Ecol. Prog. Ser.*, *328*, 75–92. Retrieved from `http://www.int-res.com/abstracts/meps/v328/p75-92/` doi: 10.3354/meps328075

Sutton, J. N., Johannessen, S. C., & Macdonald, R. W. (2013). A nitrogen budget for the Strait of Georgia, British Columbia, with emphasis on particulate nitrogen and dissolved inorganic nitrogen. *Biogeosciences*, *10*(11), 7179–7194. Retrieved from `https://bg.copernicus.org/articles/10/7179/2013/` doi: 10.5194/bg-10-7179-2013

Svendsen, H. (1995). Physical oceanography of coupled fjord-coast systems in northern Norway with special focus on frontal dynamics and tides. In *Ecology of fjords and coastal waters: proceedings of the Mare Nor Symposium on the Ecology of Fjords and Coastal Waters, Tromsø, Norway, 5-9 December, 1994* (pp. 149–164). Amsterdam ; New York: Elsevier. (Meeting Name: Mare Nor Symposium on the Ecology of Fjords and Coastal Waters)

Thomson, R. E. (1976). Tidal Currents and Estuarine-Type Circulation in Johnstone Strait, British Columbia. *J. Fish. Res. Bd. Can.*, *33*(10), 2242–2264. Retrieved from `http://www.nrcresearchpress.com/doi/10.1139/f76-272` doi: 10.1139/f76-272

Thomson, R. E. (1981). *Oceanography of the British Columbia coast* (Vol. 56). Can. Spec. Publ. Fish. Aquat. Sci.

Thomson, R. E., & Huggett, W. S. (1980). M2 Baroclinic Tides in Johnstone Strait, British Columbia. *Journal of Physical Oceanography*, *10*(10), 1509–1539. Retrieved from `https://doi.org/10.1175/1520-0485(1980)010<1509:MBTIJS>2.0.CO;2` doi: 10.1175/1520-0485(1980)010⟨1509:MBTIJS⟩2.0.CO;2

Thomson, R. E., & Krassovski, M. V. (2010). Poleward reach of the California Undercurrent extension. *J. Geophys. Res.*, *115*(C9), C09027. Retrieved from http://doi.wiley.com/10.1029/2010JC006280 doi: 10.1029/2010JC006280

van Heijst, G. (1986). On the Dynamics of a Tidal Mixing Front. In *Elsevier Oceanography Series* (Vol. 42, pp. 165–194). Elsevier. Retrieved from https://linkinghub.elsevier.com/retrieve/pii/S0422989408710456 doi: 10.1016/S0422-9894(08)71045-6

Waldichuk, M. (1957). Physical Oceanography of the Strait of Georgia, British Columbia. *J. Fish. Res. Bd. Can.*, *14*(3), 321–486. Retrieved from http://www.nrcresearchpress.com/doi/10.1139/f57-013 doi: 10.1139/f57-013

Ware, D. M., & McFarlane, G. A. (1989). *Fisheries production domains in the Northeast Pacific Ocean.* (Can. Spec. Publ. Fish. Aquat. Sci. No. 108).

Whitney, F., Crawford, W., & Harrison, P. (2005). Physical processes that enhance nutrient transport and primary productivity in the coastal and open ocean of the subarctic NE Pacific. *Deep Sea Research Part II: Topical Studies in Oceanography*, *52*(5-6), 681–706. Retrieved from https://linkinghub.elsevier.com/retrieve/pii/S0967064505000044 doi: 10.1016/j.dsr2.2004.12.023

Supporting Information for "Tidal mixing maintains regional differences in water properties and nutrient ratios in British Columbia coastal waters"

H.V. Dosser[1], S. Waterman[1], J.M. Jackson[2], C.G. Hannah[3], B.P.V. Hunt[1,4,5]

[1]Department of Earth, Ocean and Atmospheric Sciences, University of British Columbia, Vancouver, BC, V6T 1Z4

[2]Hakai Institute, 1010 Langley St, Victoria, BC, V8W 1V8

[3]Fisheries and Oceans Canada, Institute of Ocean Sciences, Sidney, BC, V8L 4B2

[4]Institute for the Oceans and Fisheries, University of British Columbia, Vancouver, BC, V6T 1Z4

[5]Hakai Institute, Heriot Bay, Quadra Island, BC, V0P 1H0

Contents of this file

Introduction

The following Supporting Information is included herein: S.1 provides additional details regarding regional definitions, S.2 expands on the descriptions of sampling biases in the data from Section 2.2, and S.3 provides additional information about the nutrient concentration data.

Corresponding author: H. V. Dosser, Department of Earth, Ocean and Atmospheric Sciences, University of British Columbia, Vancouver, BC, V6T 1Z4, Canada. (hdosser@eoas.ubc.ca)

S.1 Study area: Definitions of regions and evidence of tidal mixing

The boundaries of our study area are chosen based on the availability of DFO, UBC, and Hakai Institute data. Within this area, we define four regions that are located within the generally accepted boundaries of Queen Charlotte Strait (QCSt), Johnstone Strait (JS), the Discovery Islands (DI), and the Strait of Georgia (SoG) (Figure 1). We restrict our focus to eastern QCSt (east of 127.4°W) due to sparse DFO and UBC data and the complete absence of Hakai Institute data in western QCSt. We focus on only the northern SoG (north of 49.8°N) due to its proximity to JS and the DI and the availability of Hakai Institute samples.

A secondary consideration when choosing our regional boundaries are the bathymetric characteristics that influence tidal mixing (Figure 1), since it is anticipated that these factors will have a critical impact on regional differences. As described in Section 3.1, we use buoyancy frequency, $N^2 = -(g/\rho)\ d\rho/dz$, where ρ is the density calculated from each set of T, S profiles and g is the acceleration due to gravity, as a proxy for the direct influence of mixing in each region (Figure 2, Figure S1). In the DI, the shallow, constricted passages are conducive to enhanced tidal mixing, reflected in the absence of significant stratification there. By contrast, the topography in the JS region is smoother and deeper, and weak stratification suggests weaker in-situ tidal mixing. QCSt and the SoG have less complex bathymetry and are more strongly stratified than JS or the DI, with the strong stratification extending to the sills between regions.

Bathymetric features such as sills provide natural boundaries between regions. We define the JS region to include only the deep western basin of Johnstone Strait, and include the shallow, weakly-stratified eastern basin on the other side of the JS/DI sill

(Figure 2) in the DI region. This choice allows the tidal mixing frontal zone to span the boundary between the JS and DI regions. Within the DI, we exclude passages near Bute Inlet, as the high volume of freshwater outflow results in properties that differ from the rest of the region. Lastly, for the SoG region, we include strongly-stratified locations to the east of Quadra Island, terminating at the shallow sills entering the passages between islands in the DI.

S.2 Sampling biases

Both seasonal and spatial sampling biases present in the combined data product reflect the difficulty of sampling in challenging conditions, while interannual and depth biases reflect institutional and technical limitations.

Interannual bias: Temperature and salinity data prior to the mid-1940s are extremely limited. A marked increase in sampling in JS, QCSt, and the DI during the late 1970s was driven in large part by the efforts of a single DFO research program (see e.g. Thomson, 1976; Thomson & Huggett, 1980; Thomson, 1981), which was followed by a decrease in sampling during the 1980s and early 1990s. Few nutrient concentration data exist prior to 1998 in any region (Figure S2). The sharp increase in T, S, and nutrient data after 2014 corresponds to the beginning of the Hakai Institute sampling program. There is a significant interannual bias to recent years in all regions.

Seasonal and spatial biases: Seasonal bias is linked to spatial bias, in that DFO routinely samples repeat stations during particular months of the year (e.g. once in May and once in September), while the Hakai Institute only samples in JS and QCSt from April to July. Sampling is biased towards the summer months in all regions due to the difficulty of accessing remote stations during winter conditions (Figure S3). Since DFO, UBC, and the Hakai Institute all prioritize sampling at repeat stations, data are also biased to these locations. Despite this, T-S profiles are available at locations that span most of each region during all seasons (Figure 3, map). The DI region has the lowest spatial density of sampling locations, while the SoG has the highest. In the DI, the number of sampling locations is lower in channels with extremely strong tidal currents due to the difficulty of making measurements in such conditions. The spatial coverage of nutrient concentration data is even sparser (Figure S4). There are only two Hakai nutrient sampling stations in QCSt, both near the JS sill. In the DI, most of the DFO nutrient samples are taken near Chatham Point and along Nodales Channel, while Hakai nutrient samples are taken along the eastern side of Quadra Island. In the SoG, much of the DFO nutrient data comes from several repeat stations to the south of Discovery Passage, while the Hakai nutrient sampling stations are located near Quadra Island.

Depth bias: During the earliest part of the data record, temperature and salinity samples were collected at discrete and often widely separated depths (e.g. every 50 m in the vertical), rather than as a near-continuous profile as is the case with CTD measurements. Despite this, the vast majority (93%) of T, S data have a vertical resolution of less than 2 m. Nutrient samples are typically closely spaced in the upper 10 m of the water column and more widely spaced below, with 82% of all nutrient data having a vertical resolution of less than 25 m. Since CTD data are unreliable at the surface, and since 30% of T-S profiles begin between 2 m and 10 m, we exclude T, S data in the uppermost 10 m from the analysis. Finally, both T-S and nutrient profiles often terminate well above the seafloor in the deepest passages (particularly in JS), resulting in fewer data points in the deep water column. In the case of JS, the lower portion of the water column is nearly homogeneous (Thomson, 1976, 1981), so that the paucity of full-depth profiles is not expected to significantly bias the results.

S.3 Nutrient concentrations

As described in Section 3.4, distributions of nitrate+nitrite, phosphate, and silicate concentrations (Figures S5, S6, S7) show clear regional differences, with QCSt and JS exhibiting lower median nutrient concentrations compared to the SoG and DI. All three nutrients show occasional depletion near the surface in the SoG, but concentrations are otherwise rarely limiting. Nutrient concentrations are similar in the upper ($<$50 m depth) and lower ($\geq$50 m depth) water column in JS and the DI, likely due to the influence of tidal mixing in those regions. In contrast, nutrient concentrations tend to be higher in the lower water column in QCSt and the SoG. This is likely due to nutrient replenishment by seasonal upwelling and remineralization in the lower water column, as well as nutrient utilization by phytoplankton in the upper water column, as discussed in Section 4.2.

References

Thomson, R. E. (1976). Tidal Currents and Estuarine-Type Circulation in Johnstone Strait, British Columbia. *J. Fish. Res. Bd. Can.*, *33*(10), 2242–2264. Retrieved from `http://www.nrcresearchpress.com/doi/10.1139/f76-272` doi: 10.1139/f76-272

Thomson, R. E. (1981). *Oceanography of the British Columbia coast* (Vol. 56). Can. Spec. Publ. Fish. Aquat. Sci.

Thomson, R. E., & Huggett, W. S. (1980). M2 Baroclinic Tides in Johnstone Strait, British Columbia. *Journal of Physical Oceanography*, *10*(10), 1509–1539. Retrieved from https://doi.org/10.1175/1520-0485(1980)010<1509:MBTIJS>2.0.CO;2 doi: 10.1175/1520-0485(1980)010⟨1509:MBTIJS⟩2.0.CO;2

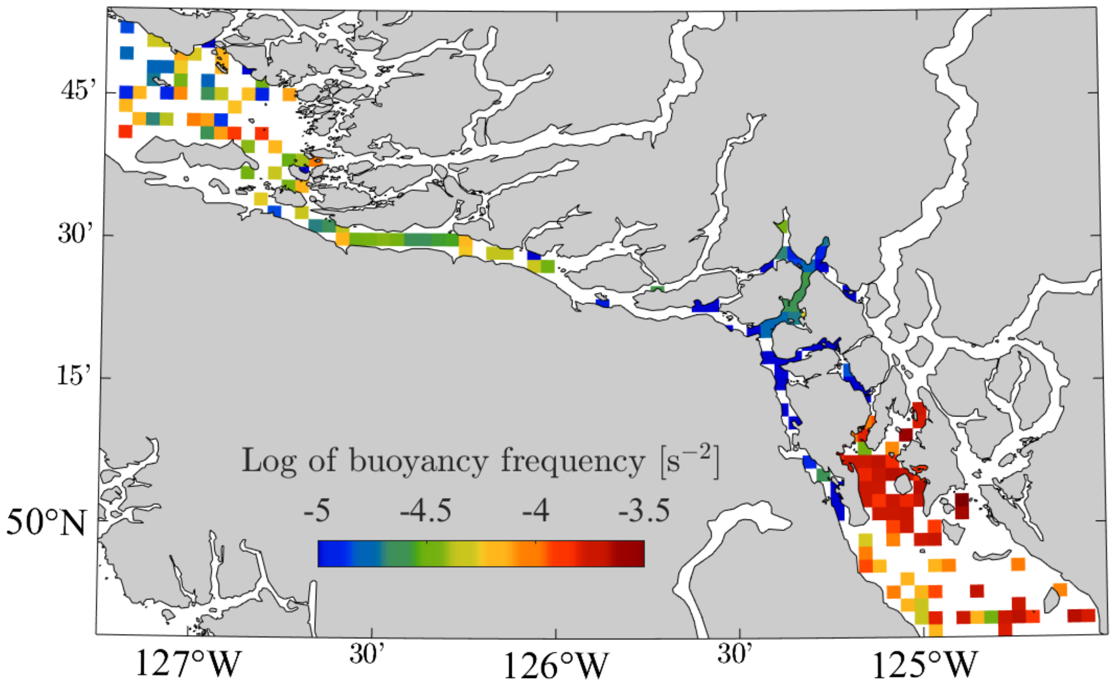

Figure S1. Identical to Figure 2, but for stratification in the winter months (November to April).

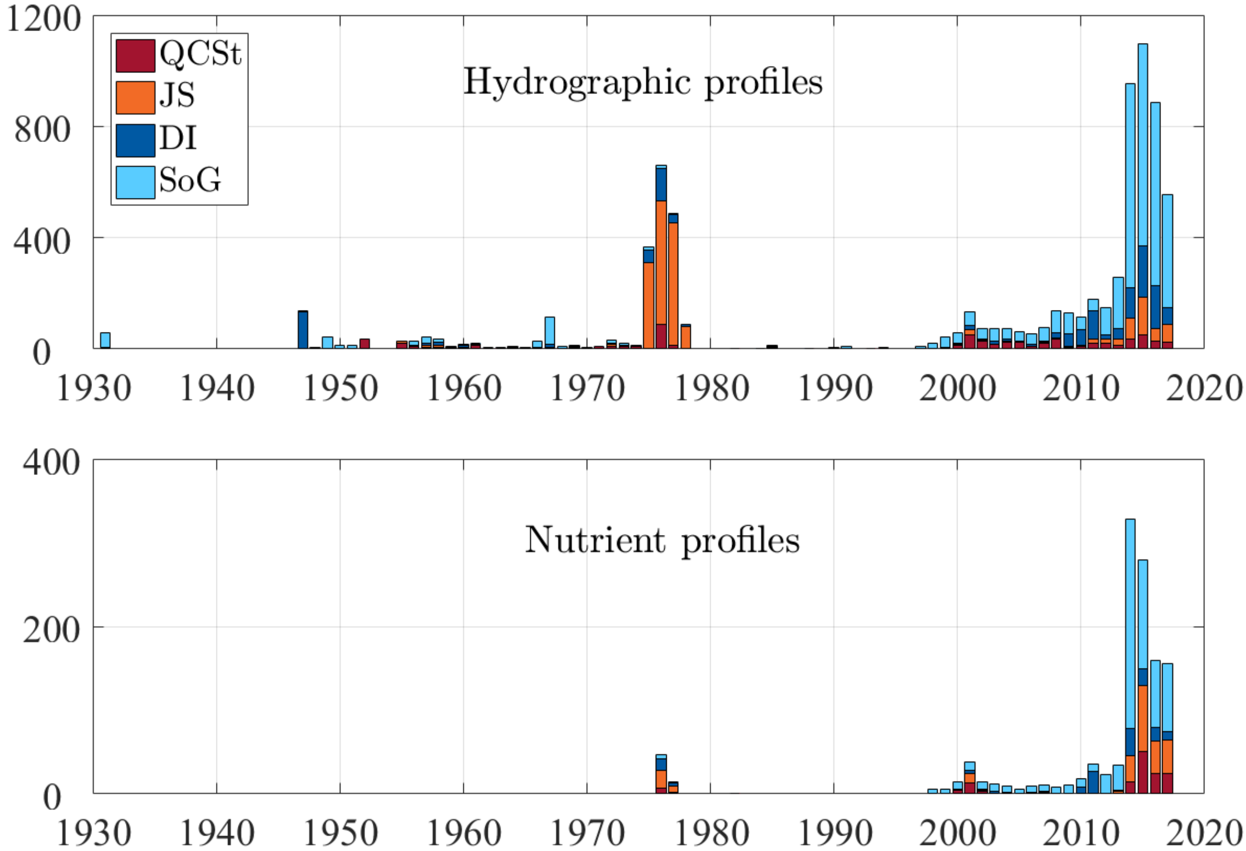

Figure S2. (Top) Number of T-S profiles collected by DFO, UBC, and the Hakai Institute each year from 1932-2018. Colours correspond to each of the four regions in Figure 1. (Bottom) As above, but for nutrient profiles, where each 'profile' includes samples of nitrate, phosphate, and silicate.

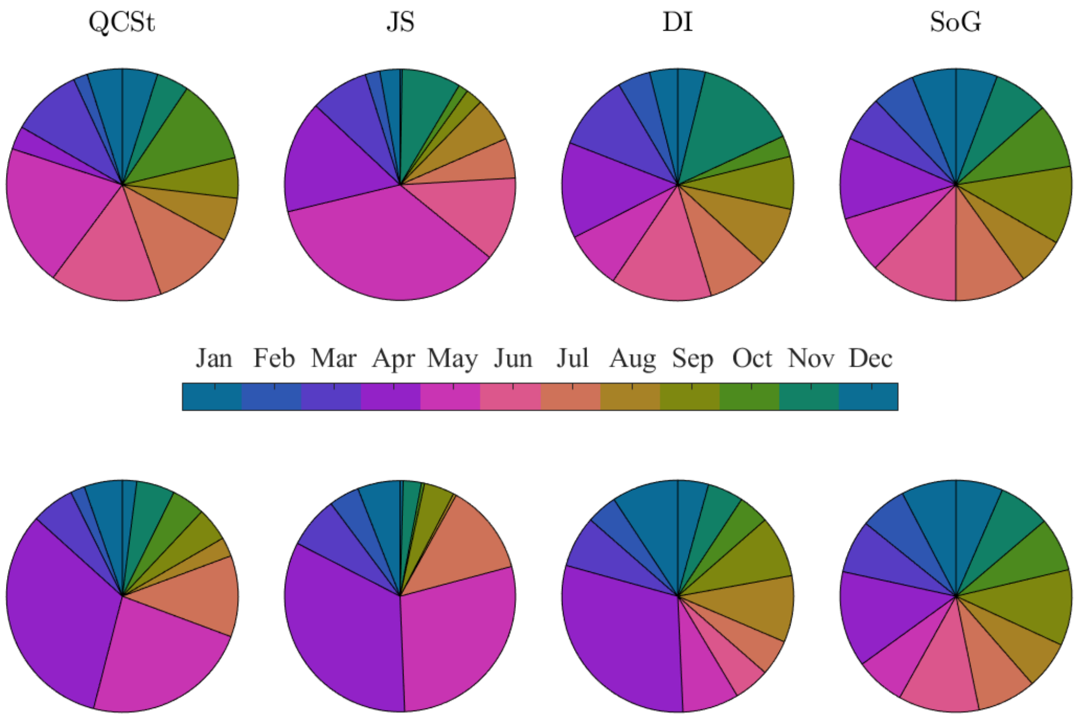

Figure S3. Fraction of total T-S profiles (top row) and nutrient sample profiles (bottom row) collected each month in each region (columns as indicated). Warmer colours indicate the summer months.

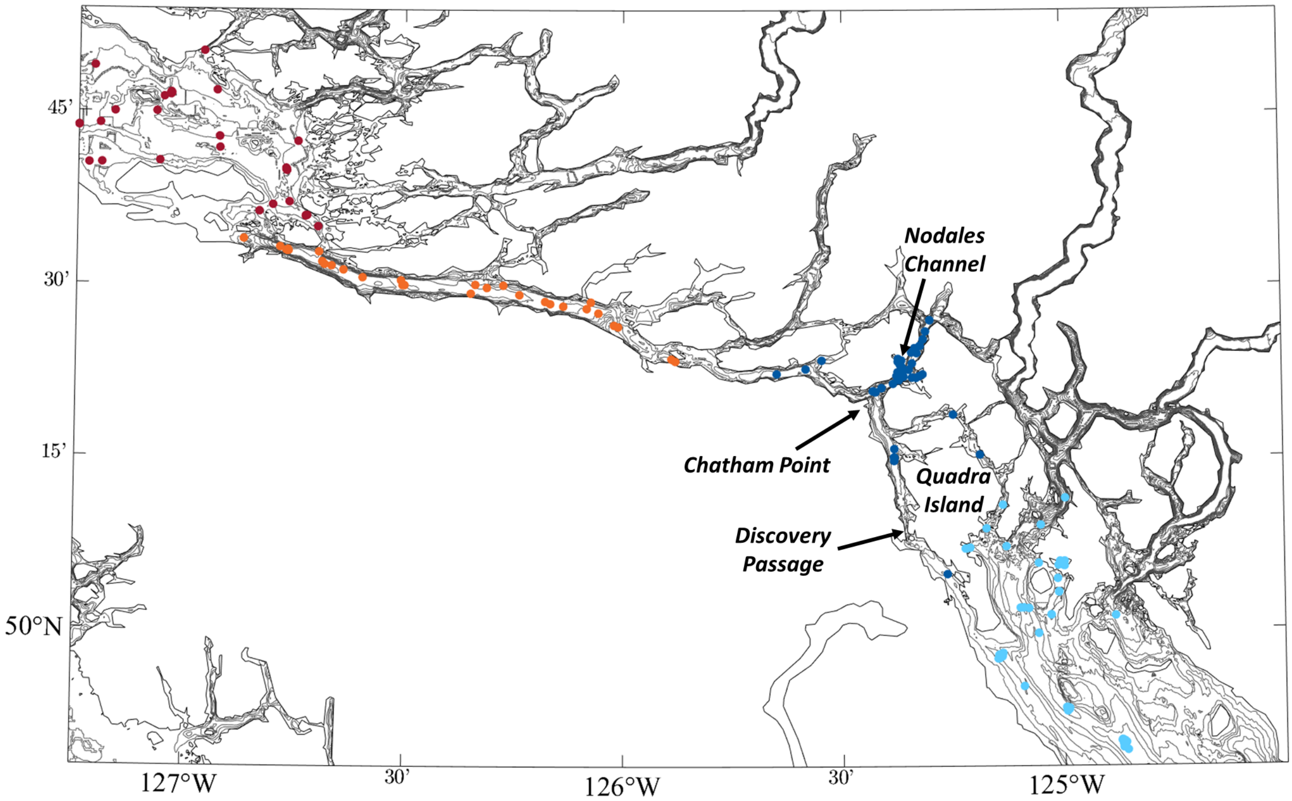

Figure S4. Bathymetric map with locations of nutrient sampling shown by the coloured dots, with QCSt in red, JS in orange, the DI in dark blue and the SoG in light blue. Locations of interest (as discussed in the text) are indicated.

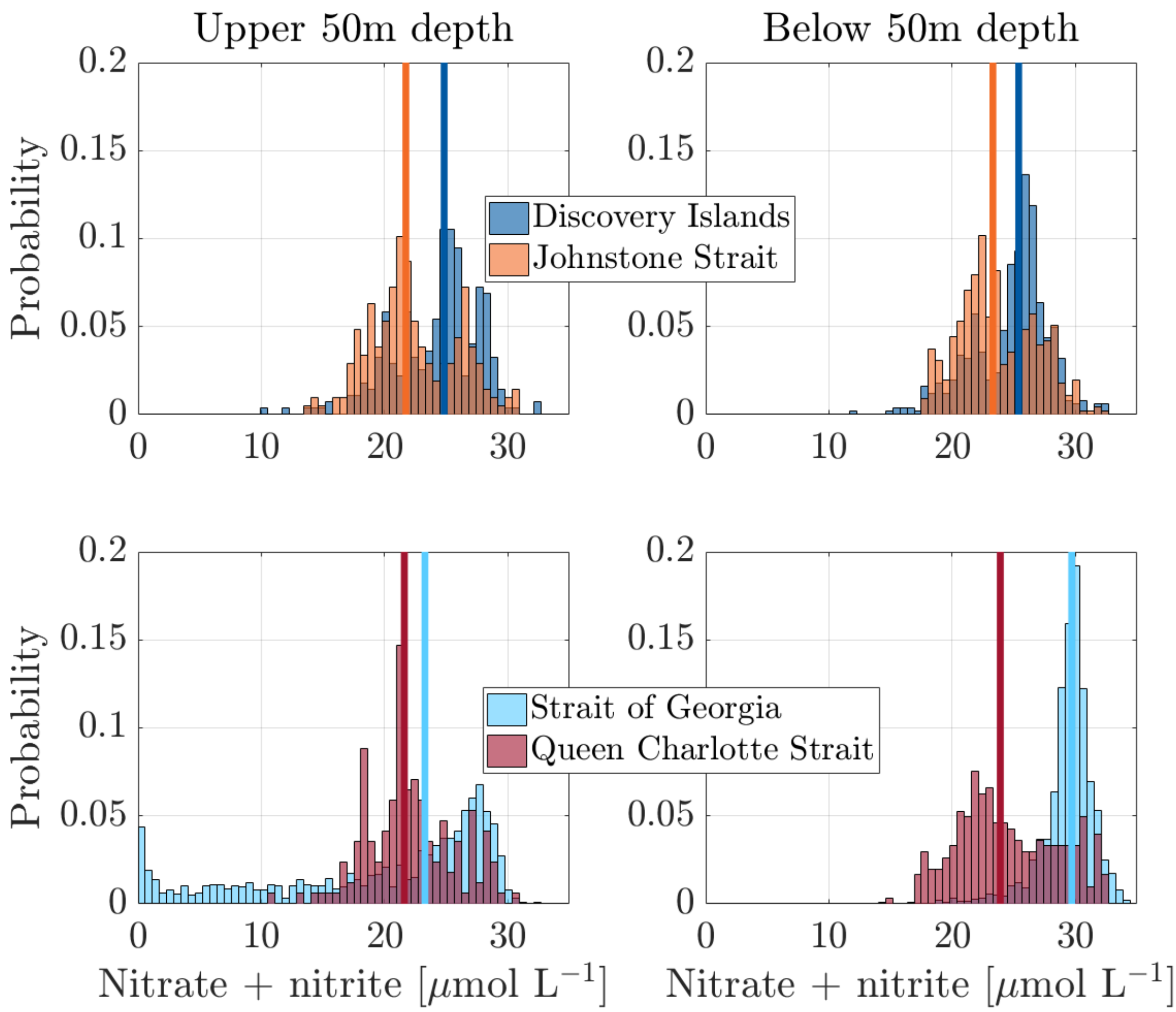

Figure S5. Distributions of nitrate+nitrite concentration, calculated using the full nutrient dataset, binned every 25 m in the vertical, and coloured by region, for the upper 50 m of the water column (left) and below 50 m depth (right). Vertical lines give the median value for each distribution.

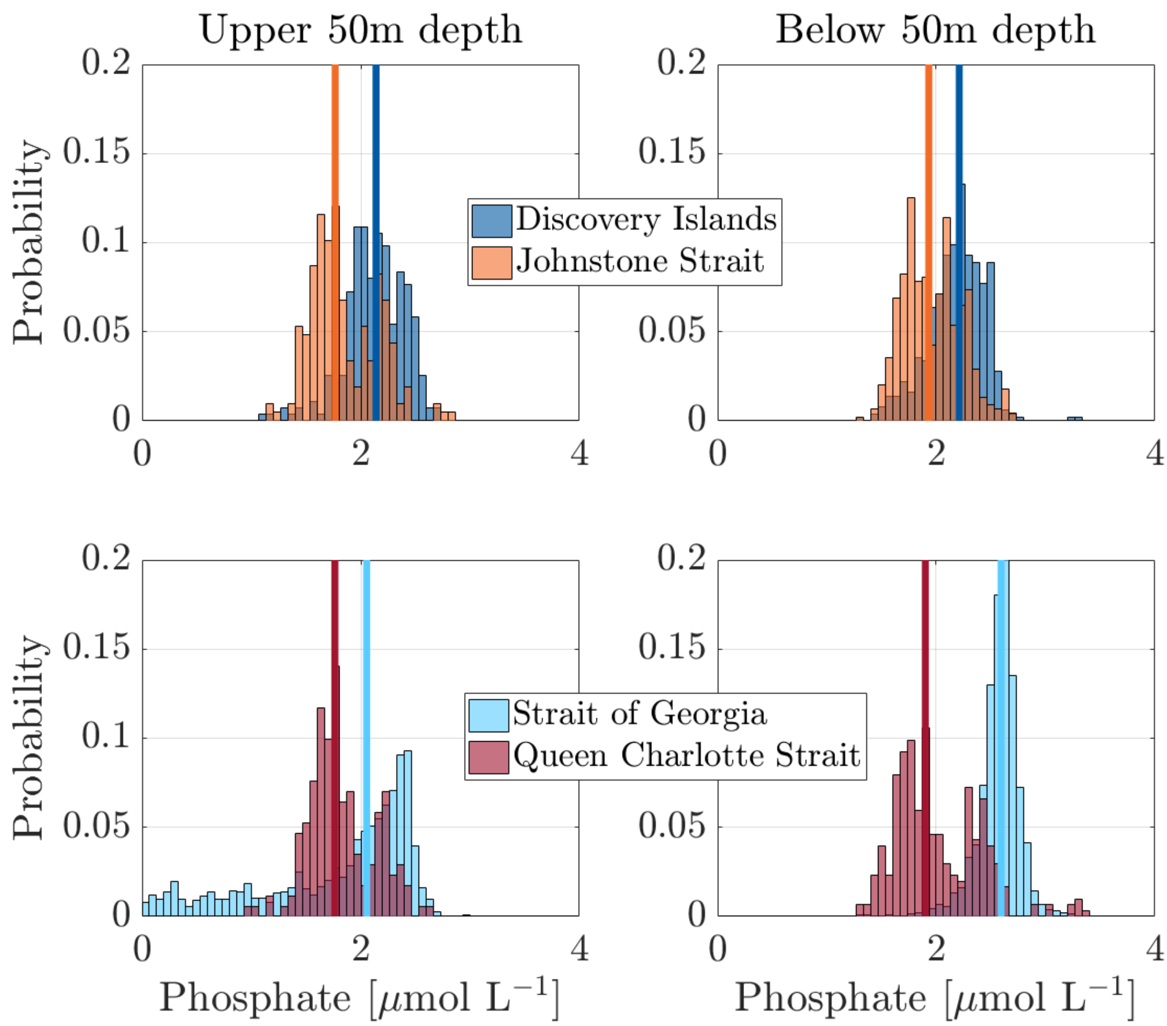

Figure S6. As in Figure S5, but for the distributions of phosphate concentration.

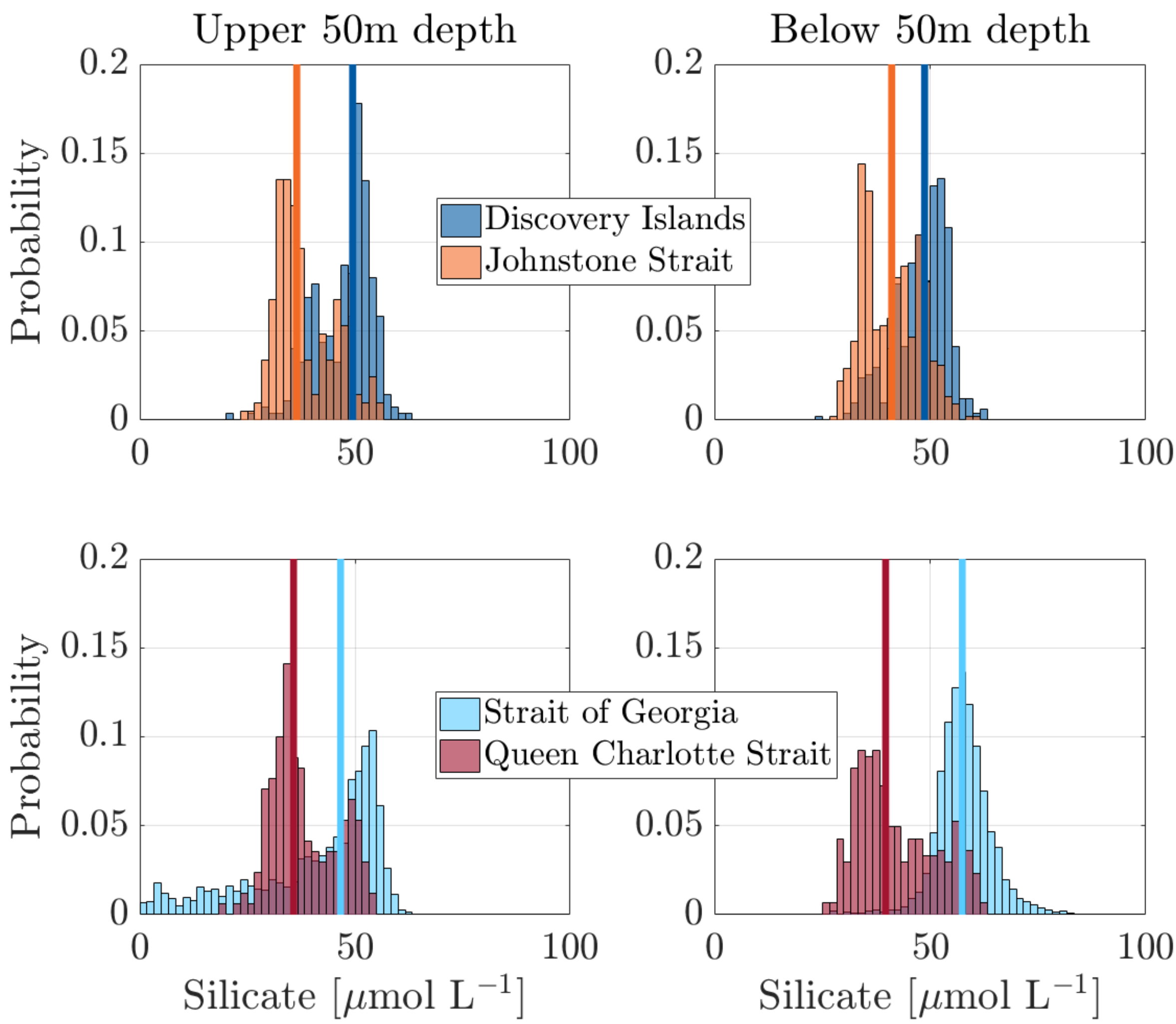

Figure S7. As in Figure S5, but for the distributions of silicate concentration.